AWARD NUMBER: W81XWH-12-1-0566

TITLE: Will PEDF Therapy Reverse Chronic Demyelination and Prevent Axon Loss in a Murine Model of Progressive Multiple Sclerosis?

PRINCIPAL INVESTIGATOR: David Pleasure MD

CONTRACTING ORGANIZATION: University of California
Davis, CA 95618

REPORT DATE: December 2015

TYPE OF REPORT: Final Report

PREPARED FOR: U.S. Army Medical Research and Materiel Command
Fort Detrick, Maryland 21702-5012

# REPORT DOCUMENTATION PAGE

*Form Approved*
*OMB No. 0704-0188*



| 1. REPORT DATE | 2. REPORT TYPE | 3. DATES COVERED |
|---|---|---|
| December 2015 | Final | 30 Sep 2012 - 29 Sep 2015 |

**4. TITLE AND SUBTITLE**

Will PEDF Therapy Reverse Chronic Demyelination and Prevent Axon Loss in a Murine Model of Progressive Multiple Sclerosis?

**5a. CONTRACT NUMBER**

**5b. GRANT NUMBER**
W81XWH-12-1-0566

**5c. PROGRAM ELEMENT NUMBER**

**6. AUTHOR(S)**

David Pleasure MD

E-Mail: depleasure@ucdavis.edu

**5d. PROJECT NUMBER**

**5e. TASK NUMBER**

**5f. WORK UNIT NUMBER**

**7. PERFORMING ORGANIZATION NAME(S) AND ADDRESS(ES)**

University of California
Office of Research
1850 Research Park Drive
Suite 300
Davis CA 95618-6153

**8. PERFORMING ORGANIZATION REPORT NUMBER**

**9. SPONSORING / MONITORING AGENCY NAME(S) AND ADDRESS(ES)**

U.S. Army Medical Research and Materiel Command
Fort Detrick, Maryland 21702-5012

**10. SPONSOR/MONITOR'S ACRONYM(S)**

**11. SPONSOR/MONITOR'S REPORT NUMBER(S)**

**12. DISTRIBUTION / AVAILABILITY STATEMENT**

Approved for Public Release; Distribution Unlimited

**13. SUPPLEMENTARY NOTES**

**14. ABSTRACT**

The purpose of this project was to assess the potential of pigment epithelium-derived factor (PEDF) as a therapy to enhance central nervous system (CNS) remyelination and preserve CNS axons in mouse models of multiple sclerosis models. After determining the dosage of recombinant PEDF required to obtain a plateau stimulatory effect on post-lysolecithin CNS remyelination, we demonstrated that intraventricular infusion of recombinant PEDF accelerated CNS oligodendrogllial recruitment from both subventricular zone neural progenitor cells and from oligodendroglial progenitor cells (OPCs), and accelerated corpus callosum remyelination. We also demonstrated that cuprizone elicited more profound corpus callosum demyelination and slower remyelination in constitutive PEDF knockout mice than in wild-type mice. In chronic experimental autoimmune encephalomyelitis (EAE) elicited by immunization with a myelin oligodendrocyte glycoprotein (MOG) peptide, intravenous, but not intraventricular, administration of PEDF diminished severity of neurological deficits.

**15. SUBJECT TERMS**

myelin, pigment epithelium-derived factor (PEDF), cuprizone demyelination, experimental autoimmune encephalomyelitis (EAE)

| 16. SECURITY CLASSIFICATION OF: | | | 17. LIMITATION OF ABSTRACT | 18. NUMBER OF PAGES | 19a. NAME OF RESPONSIBLE PERSON |
|---|---|---|---|---|---|
| a. REPORT | b. ABSTRACT | c. THIS PAGE | | | USAMRMC |
| Unclassified | Unclassified | Unclassified | Unclassified | 32 | 19b. TELEPHONE NUMBER *(include area code)* |

## Table of Contents

**Page**

**DOD Award W81XWH-12-1-0566**
**USAMRMC MS110057**
**Final Report 12/05/2015**

David Pleasure MD, Principal Investigator

**1. INTRODUCTION**: The purpose of this project was to assess the potential of pigment epithelium-derived factor (PEDF) as a therapy to enhance CNS remyelination and preserve CNS axons in mouse multiple sclerosis models.

2. **KEYWORDS**: multiple sclerosis, remyelination, pigment epithelium-derived factor (PEDF), oligodendroglial lineage

**3. ACCOMPLISHMENTS**: The Statement of Work (dated September 4, 2012) was used as the framework for organizing this report of our progress in WB1XWH-12-0566 (MS110057), updated through September 30, 2015.

**Specific Aim 1**: **To test whether PEDF therapy accelerates oligodendroglial regeneration and remyelination in corpus callosum after lysolecithin or cuprizone demyelination:**

Task 1a (*months 2-5*)—*To compare extents of remyelination in lysolecithin lesioned mice infused with different doses of PEDF and in control, saline-infused mice*.

We used myelin basic protein immunostaining to evaluate the effects in wild-type mice of recombinant PEDF lesional infusion (as contrasted with control saline infusion). By day 7 post-lysolecithin lesioning, remyelination was only partial in saline-perfused mice, but virtually complete in mice infused with 300ng/day of recombinant PEDF. The complexity of the processes of $NG2^+$ oligodendroglial progenitor cells (OPCs) was greater in the PEDF-infused mice than in saline-infused control mice (**Figure 1**). In additional studies with wild-type mice, we did not detect a significant difference between perfusion with 300ng/day and 800ng/day in rates of oligodendroglial lineage recruitment and remyelination post-lysolecithin lesioning (n=3 in each group), nor was there a significant difference between saline-perfused control mice and mice perfused with 100ng/day of PEDF (n=3 in each group) in rates of oligodendroglial lineage recruitment and remyelination. On the basis of these results, and similar results we obtained with PEDF dose-response experiments in the cuprizone demyelination model (see Task 1b, below), we concluded that 300ng/day of recombinant PEDF provides a plateau stimulatory effect on remyelination, and is an optimal dose for enhancing CNS remyelination after lysolecithin lesioning.

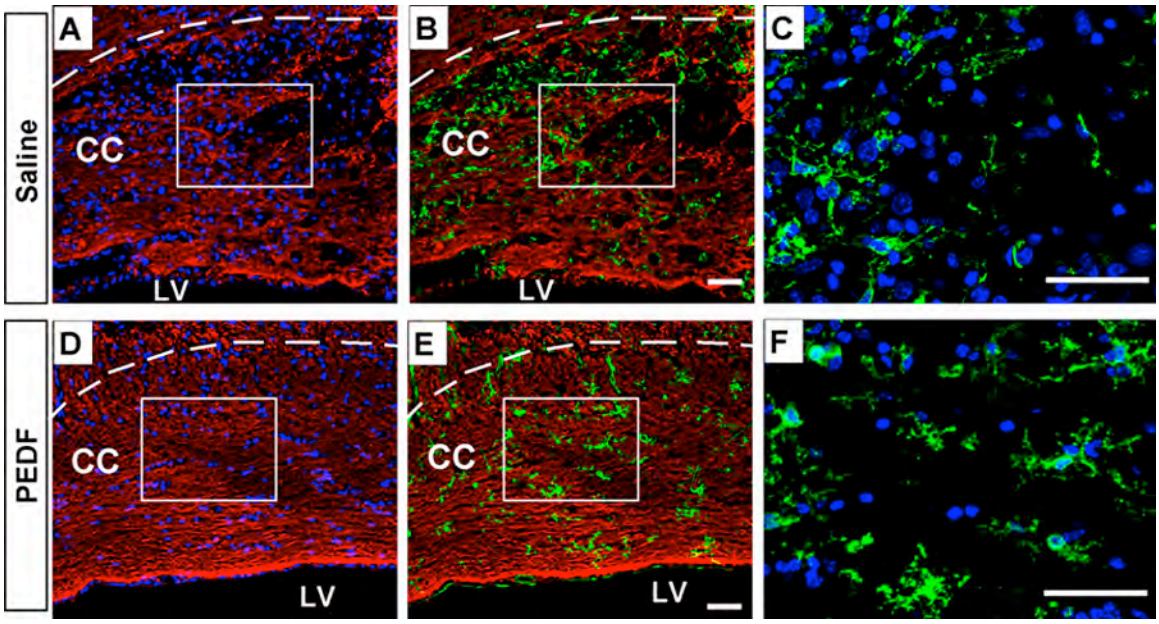


**Figure 1 legend**: Effects of recombinant PEDF infusion on oligodendroglial lineage regeneration and remyelination of lysolecithin-demyelinated corpus callosum. Mice were sacrificed 7 days after corpus callosum lysolecithin lesioning, followed by continuous perfusion with recombinant PEDF in saline (300ng/day), or with saline alone. Frozen sections through corpus callosum (CC) above lateral ventricle (LV) were immunostained for myelin basic protein (MBP, red) and for the OPC marker NG2 (green), and are shown from a control, saline-perfused mouse (Panels A, B, and C) and from a recombinant PEDF-perfused mouse (Panels D, E, and F). Note the more robust myelination in the PEDF-treated mouse. At this time-point, numbers of NG2+ OPCs were approximately equal in the PEDF treated and saline control treated lesions (see Table 1), though their processes appeared more complex in the PEDF-treated lesions.

**Table 1**: PEDF infusion into corpus callosum lysolecithin lesions accelerates recruitment of oligodendroglial progenitor cells (OPCs) and oligodendroglia

| | OPCs day 3 | OPCs day 7 | Oligodendroglia day 7 |
|---|---|---|---|
| Saline | 98 (6) | 255 (10) | 255 (14) |
| PEDF | 404 (18)** | 272 (12) | 820 (45)** |

**Table Legend**: $NG2^+$ OPCs and $CNP^+$ oligodendroglia were counted; data are numbers of labeled cells/$mm^2$, with SEMs in parentheses. ** Significantly different, $p<0.01$.

Task 1b (*months 2-5*)—*To choose the best time-points to compare remyelination in cuprizone-fed mice infused with different doses of PEDF vs control saline-infused mice*.

Using Luxol fast-blue to visualize myelin (**Figure 2**), we found that remyelination is essentially complete by 6 weeks after a 6 week course of cuprizone (0.2%, w/w) in wild-type mice not treated with PEDF.

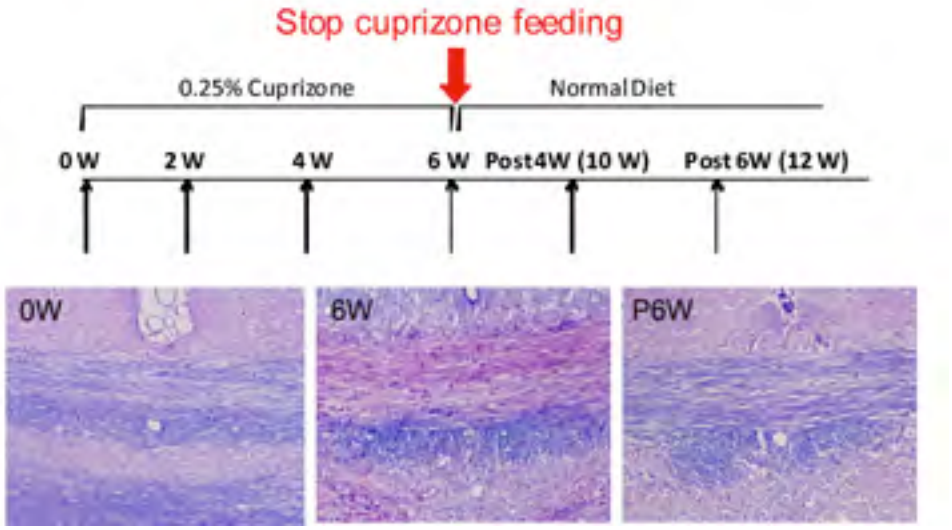


**Figure 2 legend**: Luxol fast-blue visualization of demyelination and remyelination of adult mouse corpus callosum. Adult C57BL6 mice were fed a diet containing 0.25% (w/w) cuprizone for 6 weeks, then switched back to a normal diet. Luxol fast blue shows normal myelination of corpus callosum (blue) in corpus callosum before cuprizone was started (0W), demyelination when the mice had received cuprizone for 6 weeks (6W), and return to full myelination 6 weeks post-switch back to a normal diet (P6W).

Also, in a study with wild-type mice by our lab (not supported by this grant), we documented that there is already robust recruitment of actively myelin-synthesizing immature oligodendroglia into the corpus callosum by the 6$^{th}$ week of cuprizone administration, recognizable by their expression of immunoreactive adenomatous polyposis coli (APC) (Lang et al, 2013). Numbers of these APC$^{+}$ immature oligodendroglia then fell progressively after the mice were switched back to a normal diet.

**Figure 3** shows that, during 14 days of recombinant PEDF perfusion of corpus callosum lysolecithin lesions, SVZ neural progenitor cells do give rise to nestin-fate mapped Sox10$^{+}$ oligodendroglial lineage cells, which were not detected in control mice perfused, instead, with saline.

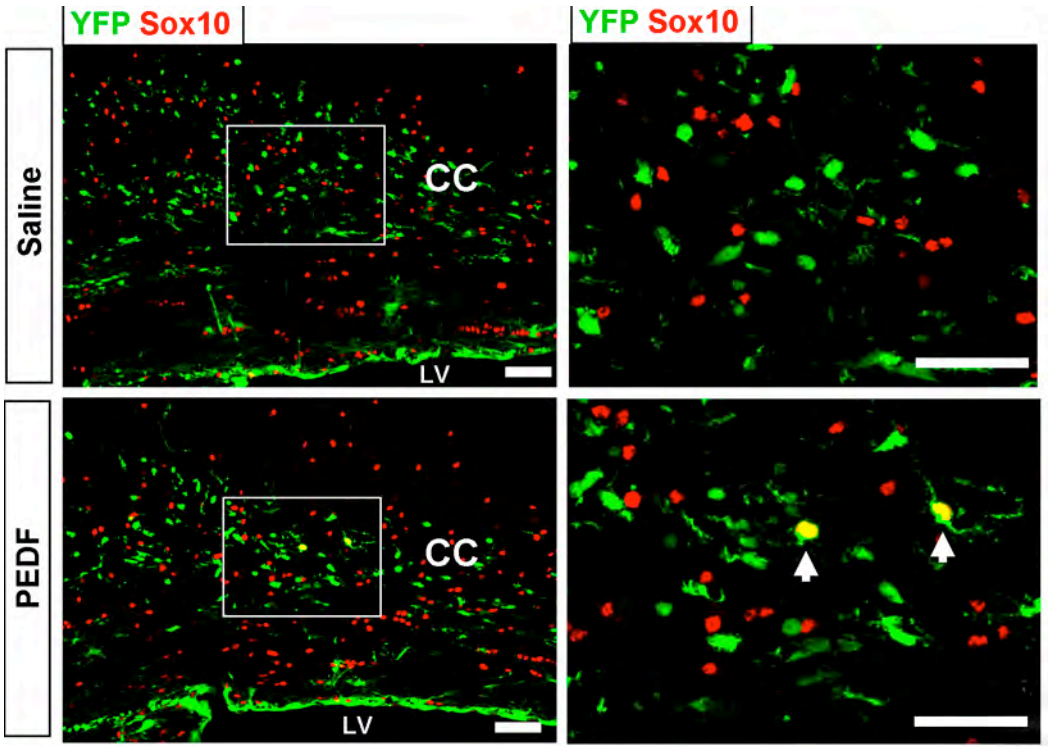


**Figure 3 legend**: Regeneration of oligodendroglial lineage cells from subventricular zone (SVZ) nestin$^{+}$ neural progenitors in recombinant PEDF-perfused corpus callosum lysolecithin lesions. Adult nestin-creER$^{T2}$/Rosa-STOP-EYFP transgenic mice were treated with tamoxifen for 5 days to induce recombination in SVZ neural progenitors. Lysolecithin lesioning of corpus callosum was performed 4 weeks later, followed by perfusion of the lesions with recombinant PEDF (300ng/day) or saline for 14 days, at which point the mice were sacrificed. Results shown are representative of 3 PEDF-treated and 3 saline-control mice. Note the presence of several fate-mapped Sox10+ cells in corpus callosum (CC) of the PEDF-treated mouse (arrowheads); these double-labeled cells were not detected in the saline perfused control mouse. However, the numbers of fate-mapped oligodendroglial lineage cells in the recombinant PEDF-perfused lesions were very small (less than 5% of total Sox10$^{+}$ oligodendroglial lineage cells) in comparison to the large effect of recombinant PEDF perfusion on overall oligodendroglial recruitment (, thus suggesting the hypothesis that most of the regenerated oligodendroglia arose from OPCs that survived within the lesion, or migrated in to the lesion from normal white matter, rather than being derived from SVZ. Size bars = 50 microns.

As in our lysolecithin studies, our cuprizone studies, performed 1 week after switching nestin-creER$^{T2}$/Rosa-STOP-EYFP mice from a cuprizone (0.2% w/w) diet back to a normal diet, showed that perfusion with 300ng/day or 800ng/day of PEDF

substantially accelerated regeneration of Sox10$^{+}$/CC1$^{+}$ oligodendroglia in corpus callosum (data not shown). We found that oligodendroglial recruitment in mice perfused with 800ng/day of PEDF is not significantly more rapid than in mice perfused with 300ng/day of PEDF, and that oligodendroglial recruitment in mice perfused with 100ng/day of PEDF is not significantly more rapid than in mice perfused with saline. These data reinforced the conclusion that we arrived at in the lysolecithin lesioning experiments that 300ng/day of recombinant PEDF is an optimal dose to accelerate remyelination after toxin-induced corpus callosum demyelination.

Our data also showed that, by day 7 post-return to a normal diet, numbers of SVZ-derived (nestin fate-mapped) cells in corpus callosum were relatively low, and that a substantial proportion of the fate-mapped cells that were present at this time-point were GFAP$^{+}$ astroglia.

Task 1c (*months 6-12*)—*To label newly formed oligodendroglia in transgenic mice treated with PEDF following corpus lysolecithin lesioning.*

Data using nestin-creER$^{T2}$-Rosa-STOP-EYFP mice to examine the effect of PEDF perfusion on oligodendroglial formation from subventricular zone (SVZ) neural progenitor cells (NPCs) after corpus callosum lysolecithin lesioning are provided under Task 1E, below.

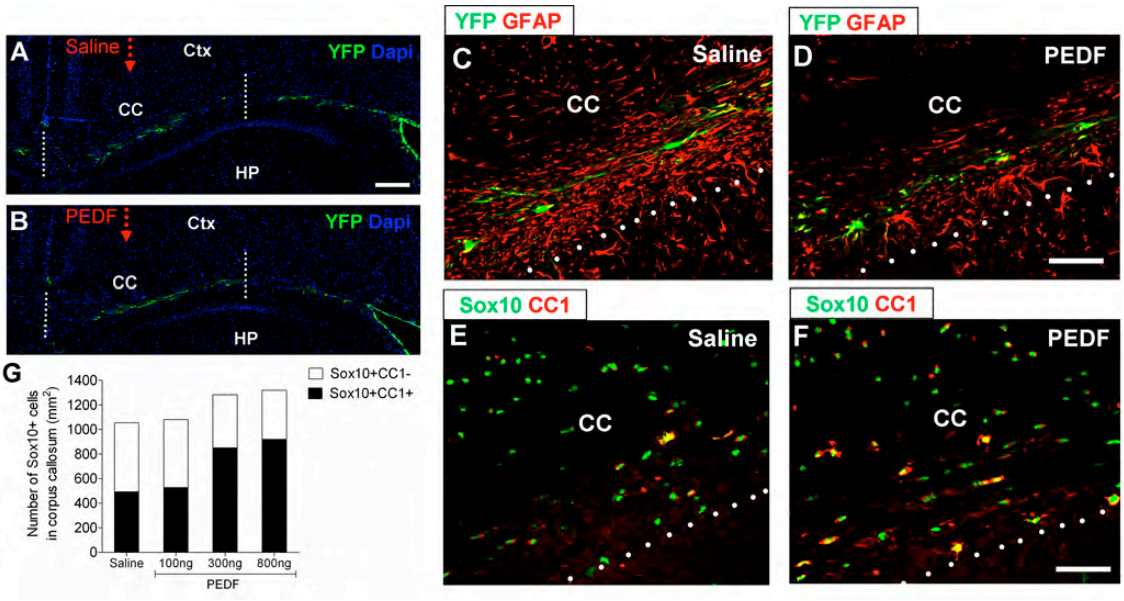


**Figure 4 legend:** Effects of 7 days of intraventricular PEDF infusion, beginning simultaneously with switching nestin-creER$^{T2}$/Rosa-STOP-EYFP mice from a cuprizone-containing diet back to a normal diet, on regeneration of oligodendroglial lineage cells in corpus callosum. Adult nestin-creER$^{T2}$/Rosa-

STOP-EYFP mice treated with tamoxifen (180mg/kg IP) daily for 5 days. Starting a week post-complection of the tamoxifen, the mice were fed an 0.2% (W/w) cuprizone diet for 6 weeks, then switched back to a normal diet. Simultaneously with the dietary switch, intraventricular perfusion was begun with PEDF in saline (100, 300, or 800 micrograms/day) or with saline alone. The mice were sacrificed 1 week later. Panels A and B show where the infusing pipettes were placed (in red) and the areas of corpus callosum that we focused on (between white dotted lines). Panels C and D show fate-mapped ($EYFP^+$) cells and $EYFP^+/GFAP^+$ cells (fate-mapped astroglia) in saline-perfused and PEDF (300ng/day) perfused mice, respectively. Note that nestin fate-mapped cells were sparse at this time-point, both in PEDF-perfused and saline-perfused mice, and that many of these fate-mapped cells were GFAP+ astroglia. Panels E and F show Sox10+ oligodendroglial lineage cells and $Sox10^+/CC1^+$ oligodendroglia in saline-perfused and PEDF (300ng/day) perfused mice, respectively. Note that numbers of $Sox10^+/CC1^+$ oligodendroglia were markedly greater in the PEDF-infused than the saline-infused mouse. Panel G shows the dose-response relationship between amount of PEDF perfused and numbers oligodendroglial lineage cells that had regenerated in corpus callosum. Because we have thus far examined only 2 mice at each PEDF dosage level, mean data are shown. Note that numbers of corpus callosum oligodendroglial lineage cells in saline-infused mice and mice infused with 100ng/day of PEDF are similar, whereas numbers of oligodendroglial lineage cells in mice infused with 300ng/day of PEDF or with 800ng/day of PEDF are almost twice those in saline-perfused mice. Size-bars = 200 microns in panels A and B, 50 microns in panels C and D.

Task 1d (*months 6-12*)—*To label newly formed oligodendroglia in cuprizone-fed transgenic mice treated with PEDF during corpus callosum remyelination.*

Results using PDGFRa-creER$^{T2}$-Rosa-STOP-EYFP mice to examine the effect of PEDF on oligodendroglial formation from oligodendroglial progenitor cells (OPCs) after corpus callosum demyelination elicited by 6 weeks of cuprizone diet are shown in **Figure 5**:

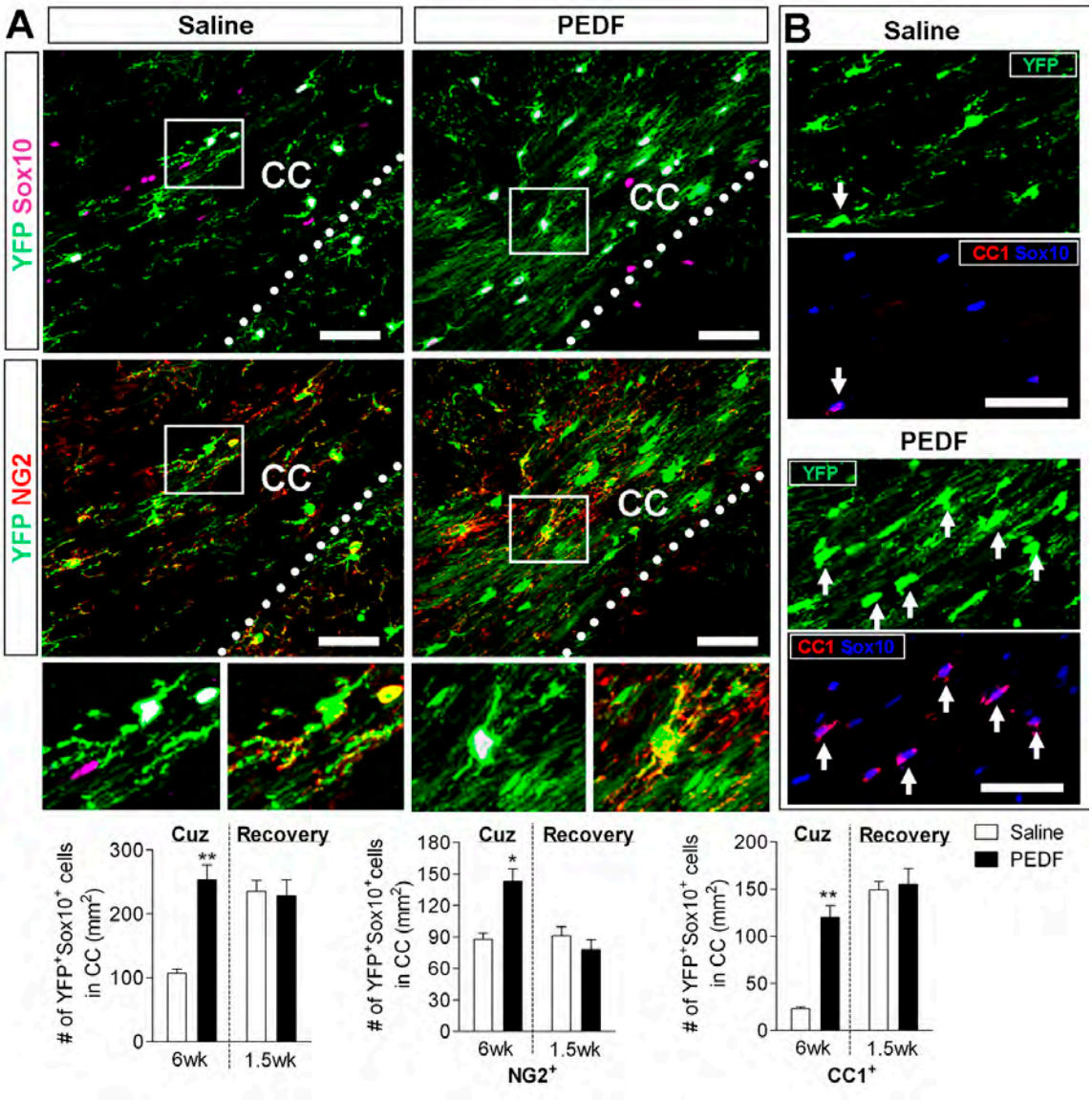


**Figure 5 legend**: Two month postnatal PDGFRa-creER$^{T2}$-Rosa-STOP-EYFP received tamoxifen injection and were then subject to cupurizone diet for 6 weeks, before switching back to a regular diet. Intracerebral perfusion via osmotic pumps of either PEDF (300ng per day) or saline begun at 4.5 weeks and continued until the mice were sacrificed at the conclusion of the cupurizone (=Cuz) diet ("6 weeks"). In another set of mice ("Recovery"), PEDF or saline infusion was initiated at the beginning of normal diet and continued for 1.5 weeks before collecting brain tissues. Both panel A and B show images taken at 6 weeks of cupurizone diet. Panel A illustrates the corpus callosum effects of the PEDF infusion on fate-mapped (green) Sox10$^+$ (pink=total oligodendroglial lineage cells) and NG2$^+$ cells (red=OPCs). The small rectangles in Panel A are shown at higher magnification below and the quantification are shown in the graphs (n=3-4 mice/group, vertical bars=SEMs, * p<0.05, **p<0.01, two-tailed Student's t-test). Note that the PEDF infusion increased the early recruitment of

OPCs (6 week time-point). Panel B and quantification demonstrate the robust effects of PEDF infusion on regeneration of corpus callosum $CC1^+$ mature oligodendroglia; substantial numbers of fate-mapped $CC1^+$ oligodendroglia had already regenerated by the end of cuprizone administration in the PEDF-perfused mice, far fewer in the saline-infused mice. In contrast, PEDF treatment during the early recovery phase (i.e., first 1.5 weeks of normal diet) did not increase the number of fate-mapped oligodendroglia in the corpus callosum. Scale bars = 50μm. Cruz = Cuprizone, CC=corpus callosum.

Task 1e and 1f (*months 12-18*)—*To label subventricular zone (SVZ) neural progenitors in transgenic mice treated with PEDF to determine their contribution to oligodendroglial regeneration and remyelination after corpus callosum lysolecithin lesioning (Task 1e) or cuprizone (Task 1f).*

For experiments with nestin-creER$^{T2}$/Rosa-STOP-EYFP (NCE) mice, tamoxifen was administered to activate the inducible nestin cre transgene prior to lysolecithin lesioning or cupurizone diet. In lysolecithin studies, fate-mapped corpus callosum $Sox10^+$ oligodendroglial lineage cells were not detected in lesional saline-perfused control mice, but were present in lesional PEDF-perfused mice (**Figure 6A**). In NCE mice fed with cupurizone for 6 week, followed by 1.5 weeks of normal diet ("Recovery"), PEDF treatment also increased the number of both fate-mapped $Sox10^+$ and CC1+ oligodendroglia in the corpus callosum as compared to saline control **(Figure 6B)**.

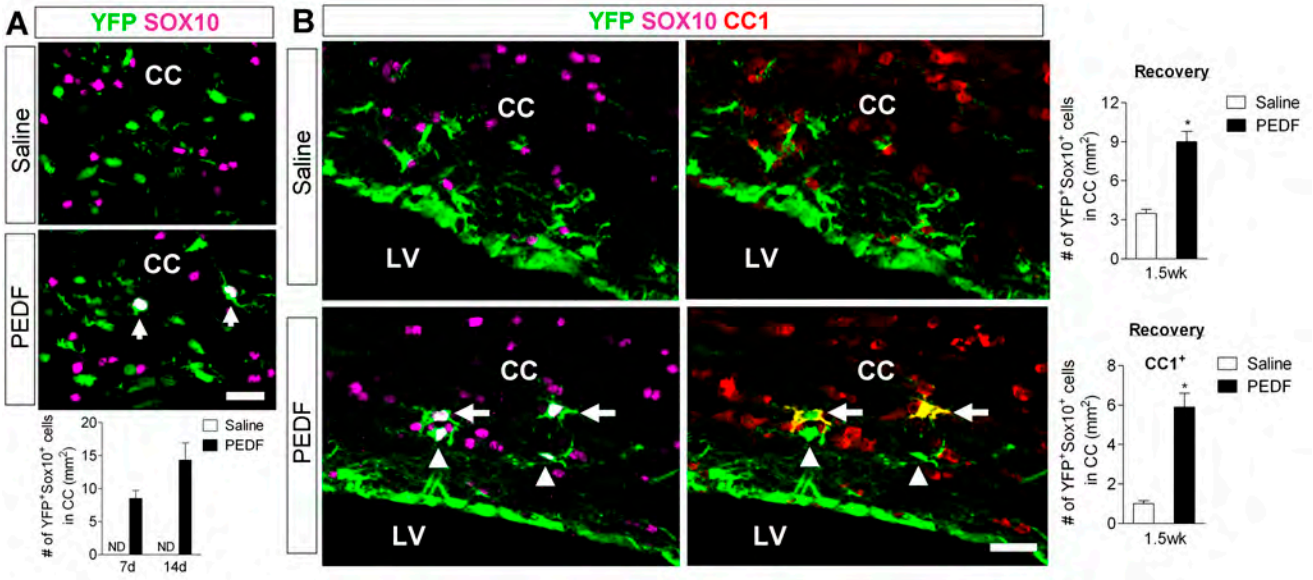


**Figure 6 legend**: PEDF enhanced regeneration of corpus callosum oligodendroglia from subventricular zone (SVZ) nestin$^+$ progenitors. Tamoxifen was administered to two month old adult Nestin-creER$^{T2}$/Rosa-STOP-EYFP mice

prior to lysolecithin lesioning or cupurizone treatment. For lysolecithin experiment (panel A), saline or PEDF was infused via osmotic pump for 7 and 14 days. For cupurizone experiment (panel B), PEDF or saline infusion was begun at the initiation of normal diet and continued for 1.5 weeks before sacrifice. Note that PEDF infusion significantly increases the numbers of corpus callosum total $YFP^+/Sox10^+$ total oligodendroglial lineage cells and $YFP^+/CC1^+$ mature oligodendroglia. Arrows indicate $YFP^+/Sox10^+$ fate-mapped oligodendroglial lineage cells in panel A and $YFP^+/Sox10^+/CC1^+$ fate-mapped mature oligodendroglia in panel B. N=3 mice in each group, vertical bars=SEM, *=$p<0.01$, Student's t-test. Size bar = 25μm. Abbreviations—CC=corpus callosum; LV=lateral ventricle.

In comparing the results shown in Tasks 1d and 1f, we concluded that the stimulatory effect of PEDF on OPC and oligodendroglial recruitment after cuprizone demyelination was more rapidly exerted on $PDGFR\alpha^+$ OPCs than on $nestin^+$ SVZ neural progenitor cells, but that both cell-types contributed to the accelerated corpus callosum oligodendroglial lineage recruitment resulting from CNS perfusion with recombinant PEDF.

Task 1g (*months 12-18*)—*To compare the oligodendroglial lineage and myelination in intact PEDF null and wild-type mice*.

Recruitment of OPCs and oligodendroglia in homozygous PEDFnull mice during early postnatal development lagged by a few days behind that in PEDF wild-type mice. At one month of age, corpus callosum myelination, as judged by myelin basic protein (MBP) immunostaining, appeared very similar in the PEDF null and littermate wild-type mice, though there were slightly fewer mature ($CC1^+$) oligodendroglia in corpus callosum of the PEDF null mice. Interestingly, as the two groups of mice aged, this deficit in numbers of corpus callosum $CC1^+$ oligodendroglia grew, and was accompanied by a diminution in corpus callosum MBP content (**see Figure 7**).

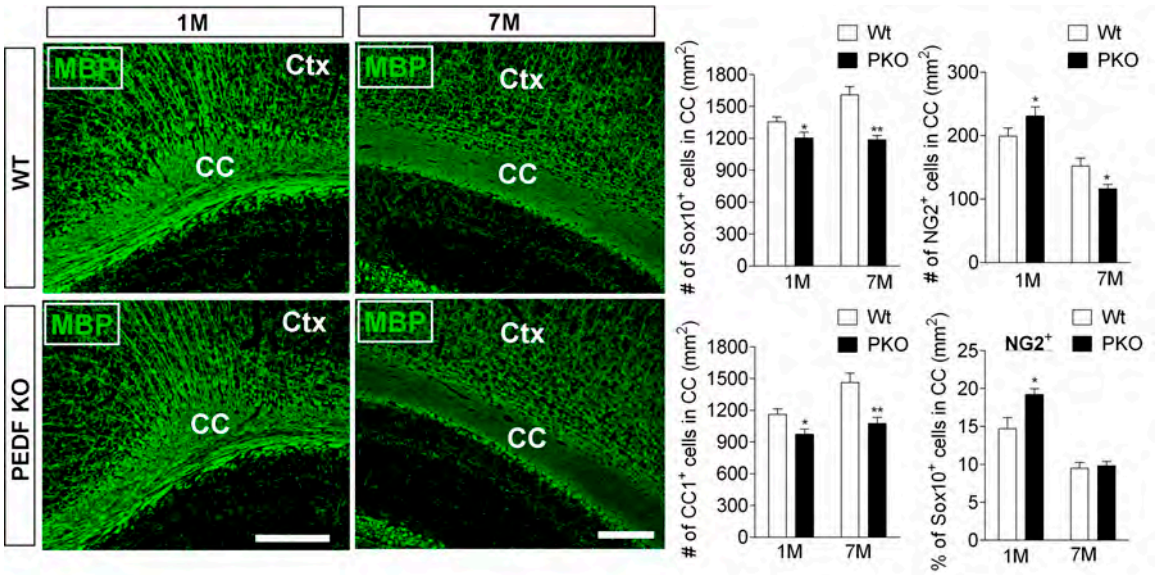


**Figure 7 legend**—Lag in oligodendroglial recruitment and myelination in PEDF KO mice. In the left immunostaining panel, immunoreactive myelin basic protein (MBP), an index of myelination, in corpus callosum was compared in 1 month postnatal ("1M") and 7 month postnatal ("7M") homozygous PEDF KO ("PEDF KO") and wild-type littermate ("WT") mice. Note that corpus callosum (CC) and overlying cortex (Ctx) myelination appeared normal at 1 month of age, but that, by 7 months of age, corpus callosum myelination was diminished in the PEDF KO mouse. Data representative of 3 mice in each group. In the right graph panel, densities (#/mm$^2$) of Sox10$^+$ total oligodendroglial lineage cells, NG2$^+$ OPCs, and CC1$^+$ mature oligodendroglia in corpus callosum in PEDF KO and wild-type littermate control mice are compared. Analyses were done on 3-4 mice of each group at each time-point, vertical bars=SEM. Note the substantial diminutions in total oligodendroglial lineage cells and of mature oligodendroglia in the PEDF KO mice at 7 months of age. *=p<0.05, **=p<0.01, Student's t-test. Size-bars =200μm.

We also compared post-cuprizone corpus callosum oligodendroglial lineage regeneration and remyelination in PEDF null and littermate control wild-type mice. When examined at the completion of 6 weeks of a cuprizone diet, there were substantially less Sox10$^+$ oligodendroglial lineage cells in corpus callosum of PEDF null than wild-type control mice, thus suggesting a protective effect of PEDF on the oligodendroglial lineage. By 1.5 weeks after the mice were returned to a normal diet, there were vigorous expansions in numbers of NG2$^+$ OPCs in both PEDF null and wild-type mice. However, by 6 weeks post-return to a normal diet, numbers of CC1$^+$ mature oligodendroglia and the level of immunoreactive MBP in corpus callosum were substantially lower in the PEDF null than wild-type mice (**see Figure 8**).

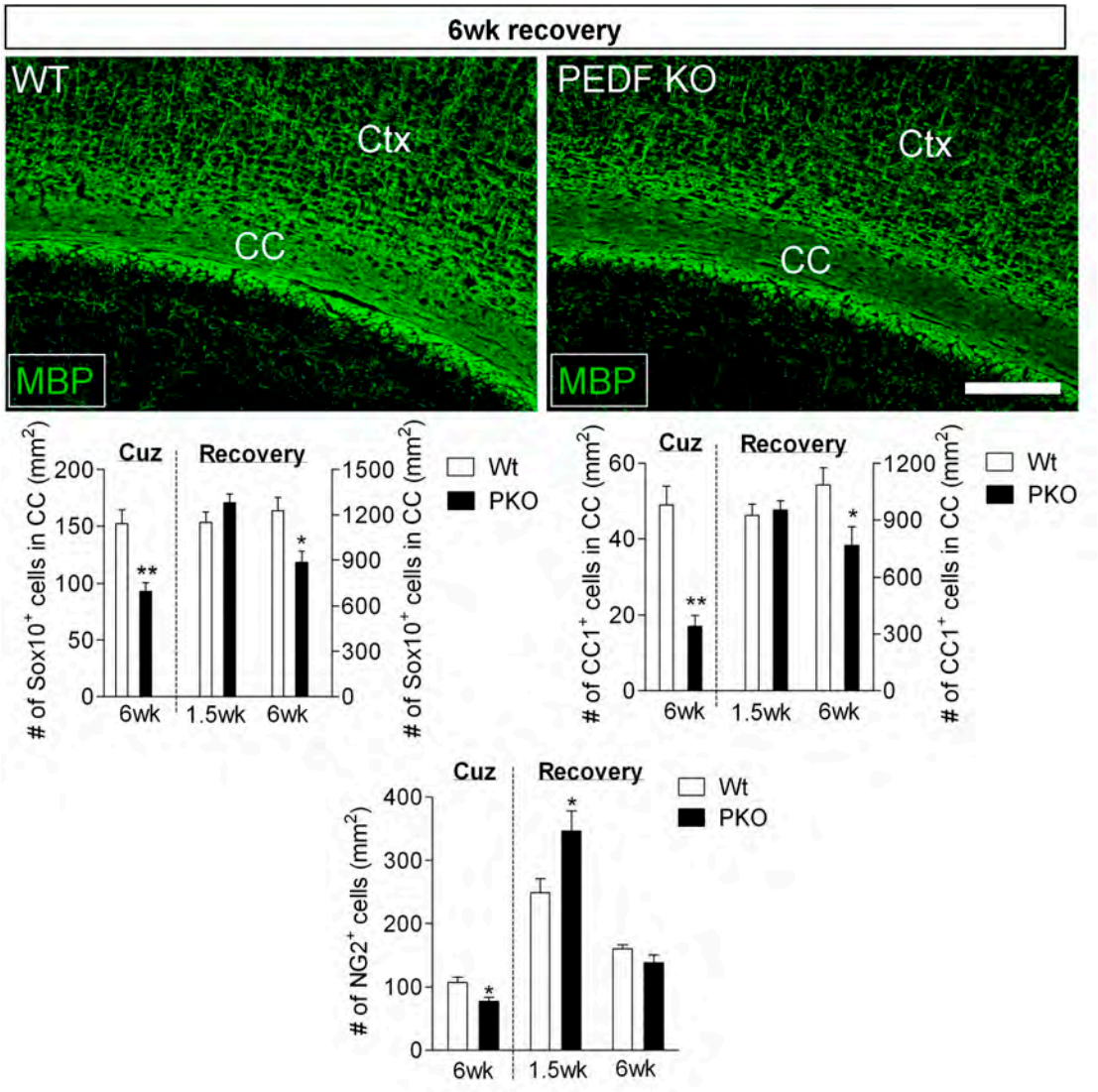


**Figure 8 legend**—Lag in remyelination after cuprizone demyelination in PEDF KO mice. MBP immunostaining shows a lesser extent of corpus callosum (CC) remyelination after 6 weeks of cuprizone followed by a 6 week recovery period on a normal diet in homozygous PEDF KO mice than in wild-type littermates. The graphs below compare numbers of corpus callosum Sox10$^+$ total oligodendroglial lineage cells, CC1$^+$ mature oligodendroglia, and NG2$^+$ OPCs in the wild-type littermate controls ("Wt") and homozygous PEDF KO ("PKO") mice at the end of the cuprizone diet, and 1.5 and 6 weeks following return to a normal diet. Note the more severe initial depletion of oligodendroglial lineage cells in the PEDF KO mice (at 6wk of cupurizone diet), the "overshoot" increase in OPCs in the PEDF KO mice 1.5 weeks after return to a normal diet, and the failure, late in recovery, of the PEDF KO mice to maintain normal numbers of CC1$^+$ mature oligodendroglia in corpus callosum. Three to four mice in each group, vertical bars=SEM, *=p<0.05, **=p<0.01, Student's t-test. Size bar = 200μm

Task 1h (months 12-18)—*To evaluate the effects of PEDF on CNS cells in tissue culture*.

This task was completed during the time interval between our initial grant application and the time we were notified that the grant had been funded. That study, which demonstrated that PEDF enhanced oligodendrogenesis from wild-type adult mouse SVZ neurospheres, was published by our laboratory in 2012 (Sohn J et al, "PEDF is a novel oligodendrogenic morphogen acting on the adult SVZ and corpus callosum, J Neurosci 32:12152-12164, 8/12 (PMID: 22933798).

We documented a lag in initial recruitment of OPCs and oligodendroglia into corpus callosum of day 4 postnatal PEDF null C57BL/6 mice, in comparison to day 4 postnatal wild-type C57BL/6 mice, but adult PEDF null corpus callosum oligodendroglia and myelin were present at normal levels.

**Specific Aim 2**: **To test whether PEDF therapy enhances remyelination and diminishes axon loss in the spinal cords of mice with MOG peptide EAE**.

Task 2a (*months 2-12*) To determine effects of IV PEDF in mice with MOG peptide EAE.

At the time we submitted this grant application, we had conducted a longitudinal assessment of the impact of IV administration of 500ng/day of recombinant PEDF from day 8 (the day of onset of neurological deficits) to day 40 post-MOG peptide immunization on the clinical evidences of MOG peptide EAE, showing that the PEDF therapy delayed the onset and decreased the peak and long-term severity of neurological deficits. We have now commenced an examination of the effects of this regimen of PEDF therapy on long-term spinal cord axon survival. Our results are shown in **Figure 9**, demonstrating, importantly, that IV PEDF therapy significantly diminishes the loss of spinal cord dorsal funiculus axons (including dorsal corticospinal tract axons) in mice with MOG peptide EAE.

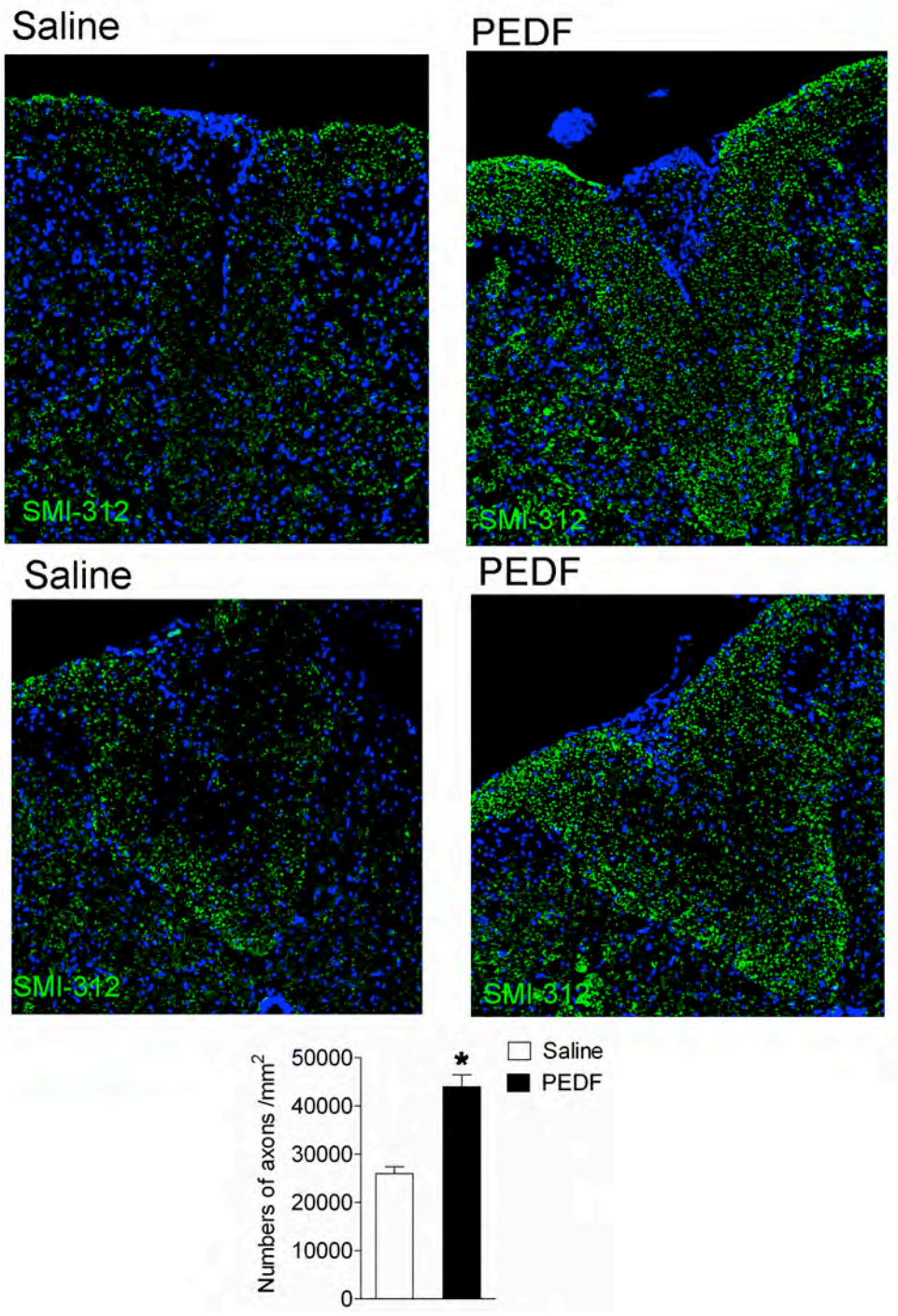


**Figure 9 legend**: IV PEDF diminishes axon loss in spinal cord dorsal funiculi (including dorsal corticospinal tracts and ascending axons of dorsal root ganglion sensory neurons) of mice with MOG peptide EAE. Lumbosacral spinal cord cross-sections from IV PEDF-treated (day 8-40 post-MOG peptide immunization) and 2 IV saline (day 8-40 post-MOG peptide immunization) control EAE mice. The mice were sacrificed on day 60 post-immunization, and the sections were

immunostained with the pan-neurofilament antibody SMI312 (green). Blue = DAPI. Note much greater numbers of preserved axons in the PEDF-treated mice. Results shown in the graph are from 6 PEDF treated vs 4 saline control mice; vertical bars denote SEMs, and * indicates significantly greater numbers of axons ($p<0.01$) in the PEDF treated than saline control mice.

Task 2b (*months 13-30*)--*To evaluate intraventricular administration of PEDF via osmotic pump on clinical severity and spinal cord axonal survival and remyelination in MOG peptide EAE mice.*

Intraventricular infusion of PEDF for 2 weeks had no statistically significant effect on the severity of MOG peptide EAE (**Figure 10**). We concluded that the elevations in CNS PEDF level via intraventricular perfusion with recombinant PEDF, though showing promise in ameliorating forebrain demyelination, were not sufficient to alleviate the limb weakness, largely attributable to spinal cord lesions, in MOG peptide EAE. Thus, while IV administration of recombinant PEDF shows promise in MOG peptide EAE, intraventricular administration of recombinant PEDF appears to be ineffective in this largely spinal cord MS model.

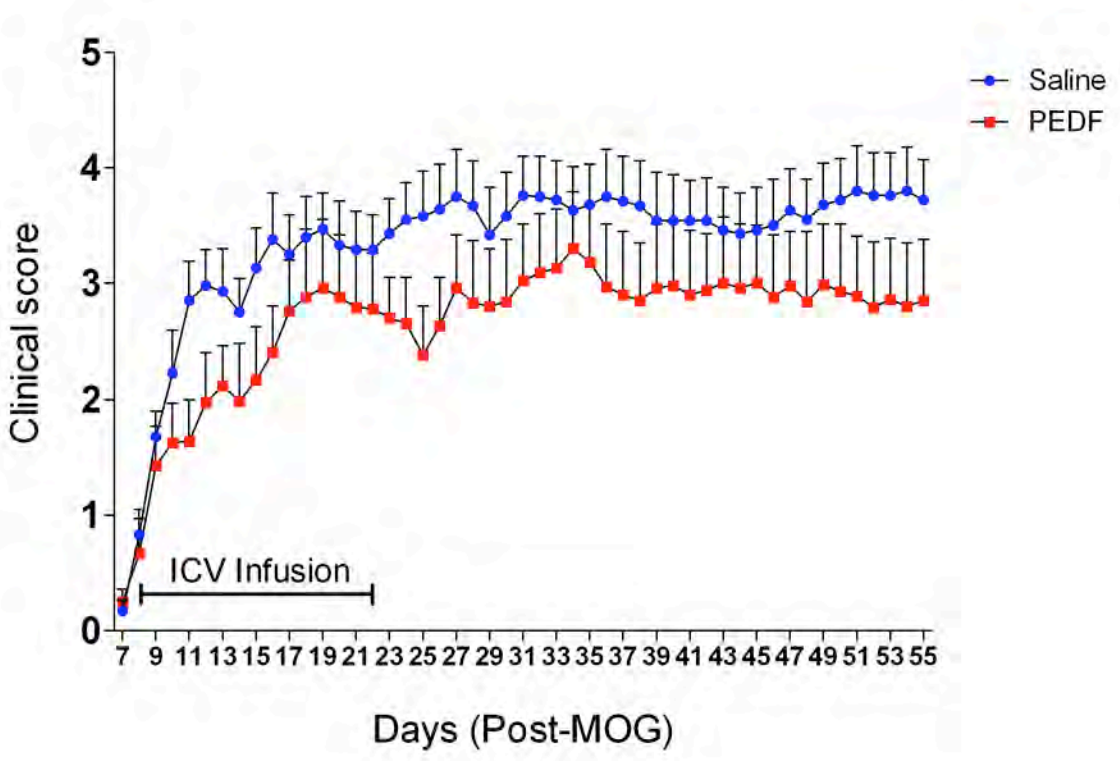


**Figure 10 legend**: Intraventricular PEDF infusion does not ameliorate clinical deficits in MOG peptide EAE. Wild-type C57BL/6 mice were intraventricularly perfused with PEDF in saline (500ng/day) or with saline alone from day 8 to day 22 post-immunization with MOG peptide in CFA. Clinical neurological exam data shown are means +/- SEMs (n=6 in each group). Differences between the

PEDF-treated and saline control mice did not reach statistical significance (Wilcoxin rank sum test).

We were also interested in determining the effects of global PEDF deficiency on MOG peptide EAE. **Figure 11** shows that MOG peptide EAE-induced clinical deficits were more severe in constitutive PEDF KO mice than in wild-type mice.

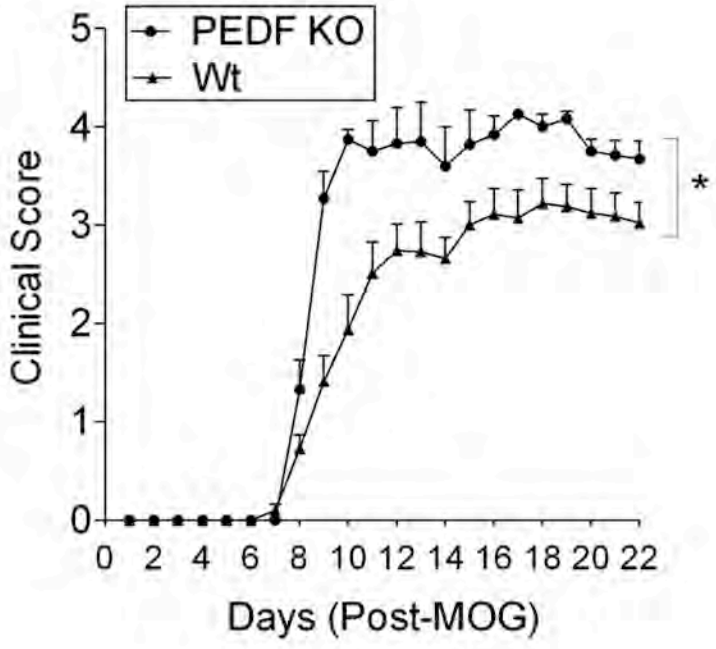


**Figure 11**—Severity of early MOG peptide EAE clinical deficits is greater in PEDF null than in wild-type mice. Six mice in each group. Vertical bars = SEMs. *significant difference between PEDF null and control mice, $p<0.05$, Wilcoxin rank sign test. A repeat study to verify this result is now underway.

Task 2c (*months 13-30*) *To evaluate forebrain administration of PEDF-adenovirus on clinical severity and spinal cord axonal survival and remyelination in MOG peptide EAE mice*.

It seemed possible that viral PEDF transduction, by inducing a greater and longer-term elevation in CNS PEDF than can be attained by intraventricular perfusion, would ameliorate MOG peptide EAE. We initiated this Task by testing the efficacy of transduction of GFP into forebrain and spinal cord by a control GFP-adenoviral vector (**see Figure 12**).

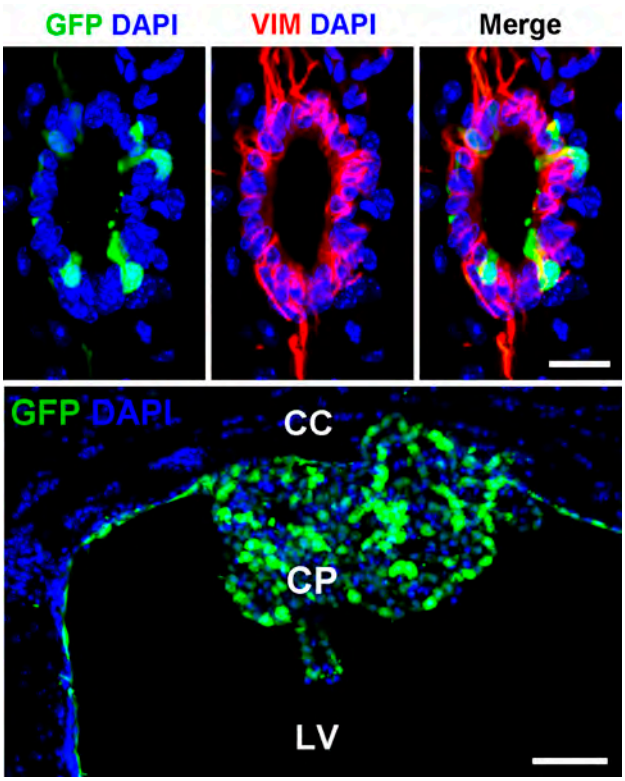


**Figure 12 legend**—A CMV promoter-driven GFP adenovirus ($5x10^7$PFU) was administered intraventricularly to a wild-type adult mouse. The mouse was sacrificed 4 days later. The upper panels show the central canal of the thoracic spinal cord, immunostained for GFP (green) and the ependymal cell marker vimentin (VIM, red), and also nuclear-stained with DAPI. Size-bar=20μm. The lower panel shows the choroid plexus of the lateral ventricle, immunostained for GFP and nuclear-stained with DAPI. Size-bar=100μm.

In subsequent experiments, however, we determined that the long-term persistence of the transduced GFP was poor, indicating that better viral vectors would be necessary for success in this Task.

Task 2d (*months 25-36*)--*To label axons in the dorsal corticospinal tracts of MOG peptide EAE mice receiving ICV infusion of PEDF.*

This Task essentially recapitulated Task 2b (see above). As mentioned above, a 2 week course of intraventricular infusion of PEDF did not ameliorate deficits in MOG peptide EAE.

Task 2e (*months 25-36*)--*To label newly formed oligodendroglia in transgenic mice with EAE treated with PEDF*.

All of the mice required for completion of this task have now been sacrificed. Histological sections have been prepared, and are currently being analyzed. We anticipate completing this post-experiment analysis, and submitting a manuscript, during the spring of 2016.

**Four additional studies highly relevant to this project are summarized here**:

1) Export of fate-mapped astroglia from the SVZ of normal adult nestin-creER$^{T2}$/Rosa-STOP-EYFP mice--We determined that numbers of astroglia in corpus callosum remain constant in normal adult mice. However, genetic fate-mapping in adult nestin-creER$^{T2}$/Rosa-STOP-EYFP mice revealed continuous generation of new corpus callosum astroglia from nestin$^{+}$ subventricular zone (SVZ) progenitor cells, thus demonstrating that the SVZ provides new astroglia to support the turnover of corpus callosum astroglia in normal adult mice. In addition, some nestin fate-mapped astroglia migrated anteriorly from the SVZ toward the olfactory bulb in association with the rostral migratory stream, but, unlike SVZ-generated neuroblasts, did not penetrate into the deeper layers of the olfactory bulb. An article reporting these observations, and citing support by DOD Award W81XWH-12-1-0566, has now been published (Sohn J et al, The subventricular zone continues to generate corpus callosum and rostral migratory stream astroglia in normal adult mice. J Neurosci 35:3756-3763, 2015, PMID: 25740506).

2) Effect of intraventricular PEDF infusion on the export of fate-mapped astroglia (EYFP$^{+}$GFAP$^{+}$) from SVZ to corpus callosum in nestin-creER$^{T2}$/Rosa-STOP-EYFP mice following corpus callosum lysolecithin lesioning—**Figure 13** shows that continuous lesional perfusion with PEDF for 7 or 14 days diminished export of fate-mapped astroglia from SVZ to corpus callosum in lysolecithin-lesioned nestin-creER$^{T2}$-Rosa-STOP-EYFP mice.

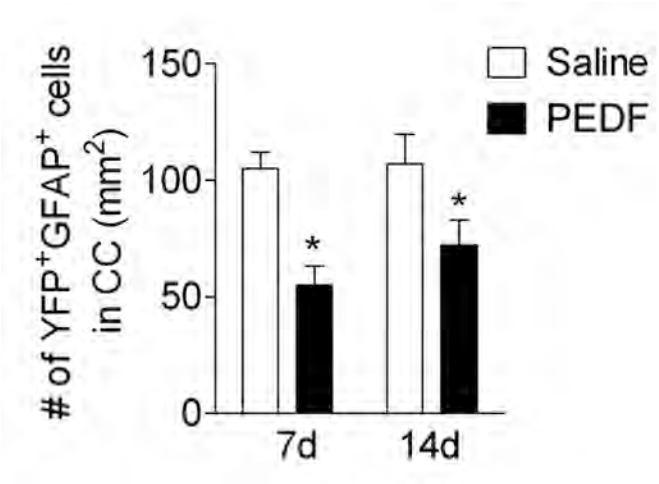


**Figure 13 legend**—Callosal lysolecithin lesions of adult nestin-creER$^{T2}$/Rosa-STOP-EYFP mice were continuously perfused with recombinant PEDF or saline. Export of fate-mapped astroglia from SVZ to corpus callosum was significantly reduced by PEDF (n=3 mice/group, $p<0.05$ at both time-points, Student's t-test).

3) Cuprizone administration causes greater injury to corpus callosum axons in PEDF KO than wild-type mice—SMI32, a monoclonal antibody that recognizes hypophosphorylated neurofilament heavy (NF-H) epitopes, does not bind to intact axons in CNS white matter, but does bind to axons in which mitochondrial metabolism and axonal transport have been perturbed. We compared SMI32 binding to corpus callosum axons in wild-type vs PEDF KO mice after 4 and 6 weeks of cuprizone diet administration, and detected substantially greater SMI32 immunoreactivity in PEDF KO than wild-type mouse corpus callosum (**see Figure 14**).

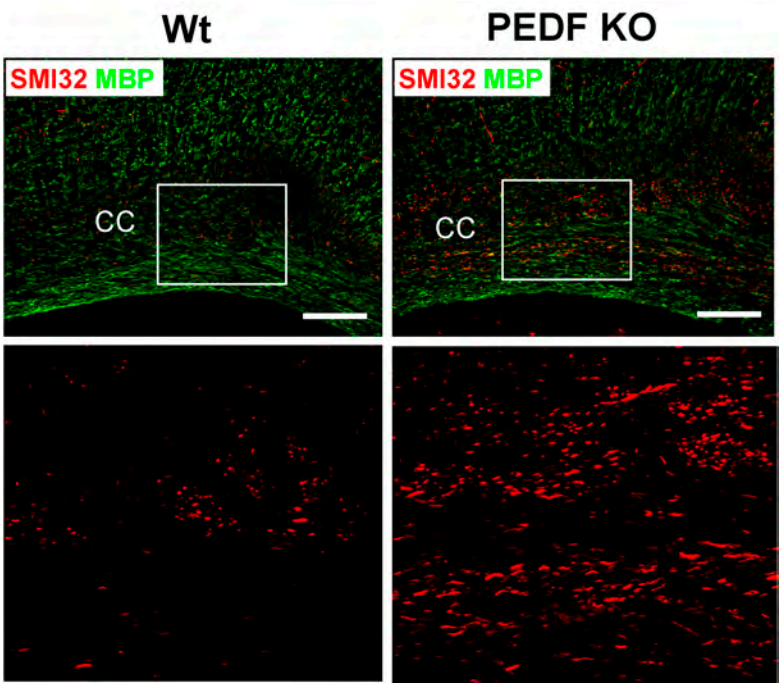


**Figure 14 legend**—Cuprizone elicits greater corpus callosum axonal damage in PEDF KO than wild-type mice, as demonstrated by SMI32 immunoreactivity at 4 weeks of cupurizone diet. Boxed areas in the upper panels are shown at higher magnification in the lower panels (size-bar=100μm).

4) Intracerebral PEDF infusion suppresses corpus callosum microglial activation in cuprizone-demyelinated mice—As previously reported by another laboratory (Remington et al, Am J Pathol 170:1713-1724, 2007), we observed marked microglial proliferation and activation in the cuprizone-demyelinated adult murine corpus callosum. Interestingly, this microglial proliferation and activation were markedly attenuated by PEDF perfusion (**see Figure 15**). Further studies of this unexpected effect of PEDF are underway in our laboratory.

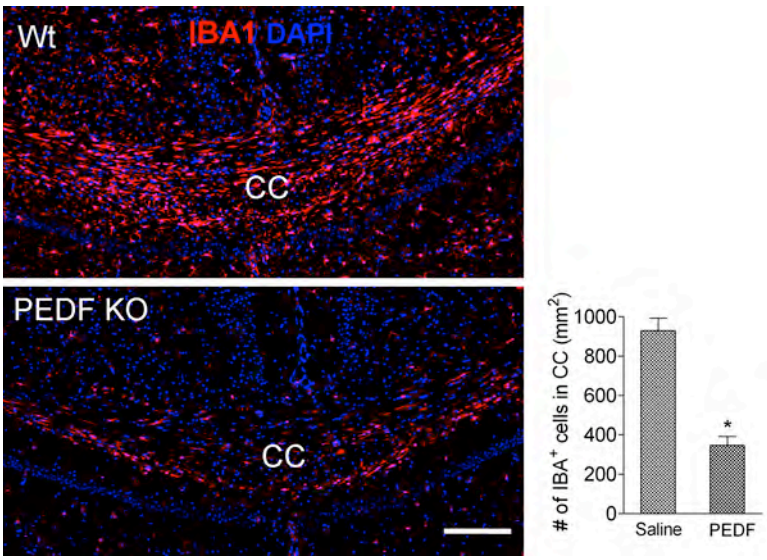


**Figure 15 legend**: PEDF decreases Iba1$^+$ microglia in corpus callosum of wild-type mice fed with cuprizone for 6 weeks, then normal diet for 10 days. Intracerebral PEDF or saline was begun at the initiation of normal diet and continued for 10 days before harvesting tissues. Size bar 100μm. Graph results with 4 mice/group. * $p<0.01$. Student t-test.

**4. IMPACT**: We used PDGFRa-creER$^{T2}$-Rosa-STOP-EYFP mice to fate-map oligodendroglial progenitor cells (OPCs) and nestin-creER$^{T2}$-Rosa-STOP-EYFP mice to fate-map subventricular zone (SVZ) neural progenitor cells (NPCs) in mice in which we had induced corpus callosum demyelination by lysolecithin (LPC) or cuprizone administration. We demonstrated that intracranial perfusion of these mice with recombinant pigment epithelium-derived factor (PEDF) enhanced regeneration of the oligodendroglial lineage and remyelination in both of these demyelinating multiple sclerosis (MS) models, and that these stimulatory effects of PEDF were exerted on both OPCs and NPCs. In a related study using nestin-creER$^{T2}$-Rosa-STOP-EYFP mice to fate-map SVZ NPCs, we demonstrated for the first time that SVZ continuously exports astroglia to the corpus callosum and rostral migratory stream (RMS) in normal adult mice.

Our experiments with intraventricular administration of adenoviral vectors demonstrated the feasibility of transduction of spinal cord ependymal and forebrain choroid plexus. However, long-term transduction efficiency was poor, indicating that more effective viral vectors would be required for success in this component of the project.

In experiments using homozygous PEDF knockout (KO) mice, we demonstrated that, while initial corpus callosum (CNS) myelination proceeded nearly as fast as in wild-type littermate controls, by age 7 months, corpus callosum of the PEDF KO mice was less heavily myelinated than that of controls, and corpus callosum content of mature oligodendroglia had fallen to below that in the controls. Also, we showed that the clinical course of experimental autoimmune encephalomyelitis (EAE) induced by immunization with myelin oligodendrocyte glycoprotein peptide 35-55 (MOG peptide) was more severe than that in wild-type littermate controls. We are now preparing a manuscript on this topic for submission for publication.

## Key Research Accomplishments

- Intracranial infusion of recombinant pigment epithelium-derived factor (PEDF) accelerates oligodendroglial regeneration from fate-mapped nestin$^{+}$ adult subventricular zone (SVZ) neural stem cells and from fate-mapped platelet-derived growth factor receptor alpha (PDGFRa)$^{+}$ oligodendroglial progenitor cells following lysolecithin- or cuprizone-induced corpus callosum demyelination

- Initial recruitment of the oligodendroglial lineage in the central nervous system (CNS) of immature mice homozygous for constitutive deletion of PEDF (PEDF KO mice) lags behind that in age-matched wild-type control mice from the same colony

- Oligodendroglial regeneration and remyelination following cuprizone-induced corpus callosum demyelination in adult PEDF KO mice lags behind that in age-matched wild-type control mice from the same colony

- Intravenous but not intracranial infusion of recombinant PEDF diminishes the clinical severity and extent of axonal loss in mice with myelin oligodendrocyte glycoprotein peptide (MOG peptide)-induced experimental autoimmune encephalomyelitis (EAE)

**5. CHANGES/PROBLEMS**: None

**6. PRODUCTS**: A Journal of Neuroscience paper by Sohn et al that was supported by this grant is appended.

**7. PARTICIPANTS & OTHER COLLABORATING ORGANIZATIONS**: David Pleasure MD, UC Davis School of Medicine

**8. SPECIAL REPORTING REQUIREMENTS**: None

**9. APPENDICES**: Sohn J, Orosco L, Guo F, Chung S-H, Bannerman P, Mills Ko E, Zarbalis K, Deng W, Pleasure D (2015) The subventricular zone continues to generate corpus callosum and rostral migratory stream astroglia in normal adult mice. J Neurosci 35(9):3756-3763 (PMID: 25740506).

Development/Plasticity/Repair

# The Subventricular Zone Continues to Generate Corpus Callosum and Rostral Migratory Stream Astroglia in Normal Adult Mice

**Jiho Sohn,[1] Lori Orosco,[1] Fuzheng Guo,[1] Seung-Hyuk Chung,[2] Peter Bannerman,[1] Emily Mills Ko,[1] Kostas Zarbalis,[1] Wenbin Deng,[1] and David Pleasure[1]**

[1]Institute for Pediatric Regenerative Medicine, University of California, Davis, School of Medicine, Sacramento, California 95817, and [2]Department of Oral Biology, University of Illinois at Chicago, Chicago, Illinois 60612

**Astrocytes are the most abundant cells in the CNS, and have many essential functions, including maintenance of blood–brain barrier integrity, and CNS water, ion, and glutamate homeostasis. Mammalian astrogliogenesis has generally been considered to be completed soon after birth, and to be reactivated in later life only under pathological circumstances. Here, by using genetic fate-mapping, we demonstrate that new corpus callosum astrocytes are continuously generated from nestin$^+$ subventricular zone (SVZ) neural progenitor cells (NPCs) in normal adult mice. These nestin fate-mapped corpus callosum astrocytes are uniformly postmitotic, express glutamate receptors, and form aquaporin-4$^+$ perivascular endfeet. The entry of new astrocytes from the SVZ into the corpus callosum appears to be balanced by astroglial apoptosis, because overall numbers of corpus callosum astrocytes remain constant during normal adulthood. Nestin fate-mapped astrocytes also flow anteriorly from the SVZ in association with the rostral migratory stream, but do not penetrate into the deeper layers of the olfactory bulb. Production of new astrocytes from nestin$^+$ NPCs is absent in the normal adult cortex, striatum, and spinal cord. Our study is the first to demonstrate ongoing SVZ astrogliogenesis in the normal adult mammalian forebrain.**

*Key words:* **astroglia; corpus callosum; genetic fate-mapping; neural progenitor cells; rostral migratory stream; subventricular zone**

## Introduction

Brain size quadruples and brain astroglial numbers increase 6- to 8-fold in normal mice and rats during the first 3 postnatal weeks (Agrawal et al., 1968; Bandeira et al., 2009; Chuang et al., 2011). There are two known forebrain origins for this rapid postnatal astrogliogenesis: (1) subventricular zone (SVZ) neural progenitor cells (NPCs) give rise to both corpus callosum and cortex astrocytes, and (2) cortical astrocytes expand themselves by symmetric divisions (Levison et al., 1993; Suzuki and Goldman, 2003; Ge et al., 2012). It has been reported, however, that, in normal circumstances, both of these astroglial recruitment mechanisms cease at the conclusion of this initial phase of rapid forebrain growth (Ling and Leblond, 1973; Sauvageot and Stiles, 2002; Ge et al., 2012), and are reactivated in adults only under pathological circumstances, for example after neural trauma (Buffo et al., 2008; Benner et al., 2013). In support of this conclusion, mitotically cycling astrocytes are rarely seen outside the forebrain neurogenic niches in normal adults (Buffo et al., 2008; Molofsky et al., 2012). But in one early study, although a 2 h systemic pulse of $^3$H-thymidine failed to label corpus callosum astrocytes in normal adult mice, labeled corpus callosum astroglial nuclei were detected by autoradiography after 30 d of continuous systemic $^3$H-thymidine administration (McCarthy and Leblond, 1988). The authors concluded that immature cells residing in the corpus callosum continued to divide and to give rise to astrocytes, but did not consider the alternate possibility that those labeled astrocytes had instead been generated from SVZ NPCs.

We have now reevaluated normal adult SVZ astrogliogenesis by genetic fate-mapping in mice carrying tamoxifen-inducible nestin-cre (nestin-creER$^{T2}$) transgene and Rosa26R-STOP-EYFP recombination marker (Lagace et al., 2007). Our results indicate that nestin$^+$ SVZ NPCs continue to generate corpus callosum astrocytes during normal adulthood, at a rate that gradually declines with advancing age. Together with our observations that: (1) overall numbers of astrocytes remain constant, and (2) astroglial apoptosis occurs in the normal adult corpus callosum, our data support the concept that there is slow, continuous turnover of astrocytes in the normal adult corpus callosum, with replacement by new astrocytes generated from nestin$^+$ SVZ NPCs. In addition, the SVZ continuously exports astrocytes to the rostral migratory stream (RMS). Unlike in the corpus callo-

Received Aug. 18, 2014; revised Dec. 15, 2014; accepted Jan. 14, 2015.

Author contributions: J.S., L.O., F.G., S.-H.C., P.B., E.M.K., K.Z., W.D., and D.P. designed research; J.S., L.O., F.G., and S.-H.C. performed research; S.-H.C. and P.B. contributed unpublished reagents/analytic tools; J.S., L.O., F.G., S.-H.C., P.B., E.M.K., K.Z., W.D., and D.P. analyzed data; J.S. and D.P. wrote the paper.

This work was supported by the Department of Defense (W81XWH-12-1-0566), Shriners Hospitals for Children, and the National Multiple Sclerosis Society (RG 5252-A-6).

The authors declare no competing financial interests.

Correspondence should be addressed to Dr David Pleasure, Institute for Pediatric Regenerative Medicine, UC Davis School of Medicine, c/o Shriners Hospital, 2425 Stockton Boulevard, Sacramento, CA 95817. E-mail: david.pleasure@ucdmc.ucdavis.edu.

DOI:10.1523/JNEUROSCI.3454-14.2015

 0270-6474/15/353756-08$15.00/0

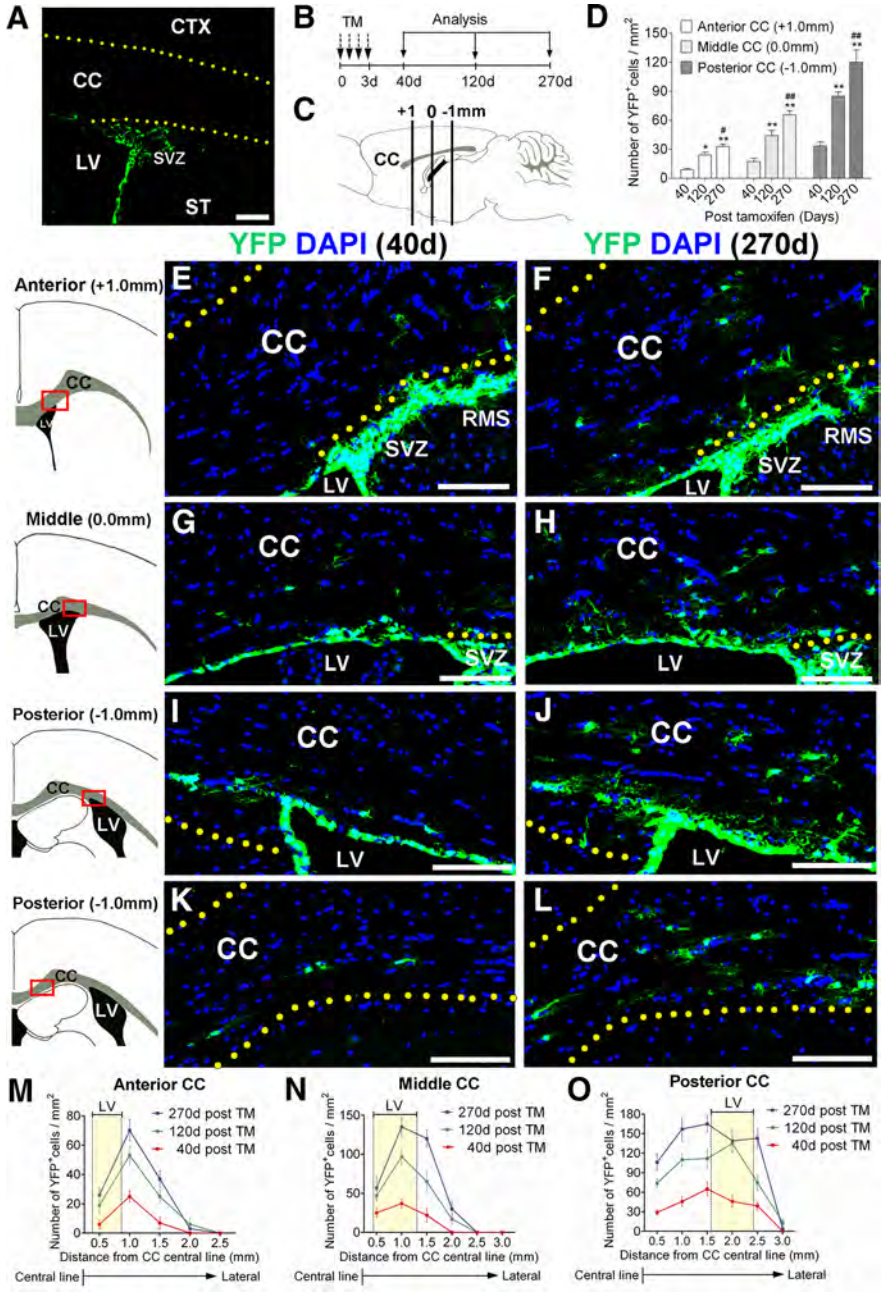


**Figure 1.** Density and distribution analyses of nestin fate-mapped cells in the adult corpus callosum. ***A***, Coronal brain section of 3-month-old NCER mice immunostained for EYFP 1 d after completion of a series of TM injections (i.p., 180 mg/kg body weight, daily for 4 consecutive days), showing EYFP$^+$ cells are restricted to the SVZ. ***B***, ***C***, Experimental design: ***B***, 3-month-old NCER mice received TM injections and were then killed at later time points (40, 120 or 270 d). ***C***, Immunohistological analysis was done on coronal brain sections at 1.0 mm anterior, 0.0 mm and 1.0 mm posterior to the bregma (anterior, middle, and posterior corpus callosum, respectively). ***D***, With increasing time post-TM injection, the density of EYFP$^+$ cells increased in all 3 anterior–posterior regions of the corpus callosum (anterior CC: $*p < 0.01$ vs 40 d, $**p < 0.005$ vs 40 d, $\#p < 0.05$ vs 120 d; middle CC: $**p < 0.005$ vs 40 d, $\#\#p < 0.01$ vs 120 d; posterior CC: $**p < 0.005$ vs 40 d, $\#\#p < 0.01$ vs 120 d). ***E–L***, Images of EYFP$^+$ cells in anterior (***E***, ***F***), middle (***G***, ***H***), and posterior (***I–L***) corpus callosum at 40 and 270 d after TM. The corpus callosum is demarcated by dotted lines. Rectangles in schematic drawings on the left mark the location of the images shown on the right. ***M–O***, Mediolateral distributions of EYFP$^+$ cells in anterior (***M***), middle (***N***), and posterior (***O***) corpus callosum. Note regional differences in mediolateral distributions of EYFP$^+$ cells in different anterior–posterior regions of the corpus callosum. In the posterior corpus callosum (***O***), EYFP$^+$ cells were more widely distributed whereas in more anterior segments (***M***, ***N***) of the corpus callosum, EYFP$^+$ cells were largely confined to the area close to the SVZ. Yellow areas in the graphs indicate mediolateral locations of the lateral ventricles. CC, Corpus callosum; CTX, cortex; LV, lateral ventricle; ST, striatum. Scale bars, 100 $\mu$m. Results are mean ± SEM ($n = 3–4$ brains).

sum and the RMS, the SVZ does not give rise to new cortical or striatal astrocytes in normal adults. Moreover, no evidence of NPC-derived astrogliogenesis is detectable in the normal adult spinal cord.

## Materials and Methods

*Animals.* C57BL/6 nestin-Cre-ER$^{T2}$ transgenic mice (Lagace et al., 2007) were crossed to C57BL/6 Rosa26R-STOP-EYFP reporter transgenic mice (The Jackson Laboratory; Srinivas et al., 2001) to yield nestin-creER$^{T2}$/R26R-EYFP (NCER) double-transgenic mice. The nestin-Cre-ER$^{T2}$ construct used in the C57BL/6 nestin-Cre-ER$^{T2}$ transgenic mice has a second intronic element that enhances nestin expression specifically in NPCs, but not in endothelial cells (Zimmerman et al., 1994; Lagace et al., 2007). GFAP:GFP transgenic mice [FVB/N-Tg(GFAPGFP)14Mes/J; Zhuo et al., 1997] were purchased from The Jackson Laboratory (stock no. 003257). GFAP:GFP transgenic mice were then crossed with C57BL/6 wild-type mice (obtained initially from the Jackson Laboratory) for >7 generations to produce GFAP:GFP transgenic mice on a C57BL/6 background. Both males and females were used in this study. All protocols used in these studies were preapproved by the UC Davis IACUC.

*Tamoxifen administration.* To genetically label nestin$^+$ SVZ NPCs, 3 month postnatal NCER mice were given intraperitoneal (i.p.) tamoxifen (TM) dissolved in 10% EtOH/90% sunflower oil (v/v) at 180 mg/kg/d for 4 consecutive days. Five days of TM at this dose had previously been reported to induce maximal genetic recombination with minimal mortality (Lagace et al., 2007), but we found that reducing administration to 4 d further lowered lethality without compromising recombination efficacy in 3-month-old NCER mice.

*Immunohistochemistry and quantification.* At the termination of experiments, the mice were anesthetized with ketamine (150 mg/kg body weight, i.p.) and xylazine (16 mg/kg body weight, i.p.), and transcardially perfused with PBS, followed by 4% paraformaldehyde (PFA) in PBS. Brain tissues were isolated and post-fixed with 4% PFA in PBS overnight at 4°C. Tissues were cryoprotected, sectioned and further immunostained as previously described (Sohn et al., 2012). TUNEL (terminal deoxynucleotidyl transferase dUTP nick end labeling) staining was performed by using DeadEnd TUNEL assay kit (Promega) following the manufacturer's instructions. Primary antibodies were as follows: anti-YFP/GFP (1:500, Abcam, Ab13970), anti-GFAP (1:500, Sigma-Aldrich G3893; Dako, Z0334), anti-Nestin (1:100, Santa Cruz Biotechnology sc-21249), anti-vimentin (1:500, Abcam, ab8979), anti-Ki67 (1:500, Abcam, ab15580), anti-EAAT1 (1:100, Abcam, Ab416), anti-EAAT2 (1:100, Abcam, Ab41621), anti-aquaporin-4 (1:50, Santa Cruz Biotechnology, Sc-20812), anti-DCX (1:50, Santa Cruz Biotechnology, Sc-8066), anti-Sox10 (1:50, Santa Cruz Biotechnology, Sc-17342), and anti-PECAM (1:50, Santa Cruz Biotechnology, Sc-18916). All fluorescent images were captured by laser scanning confocal microscopy (Nikon, C1).

For quantification (Figs. 1–4), cell counting in anterior, middle, and posterior corpus callosum was performed in coronal sections +1.0 mm, 0.0 mm, −1.0 mm with respect to the bregma, respectively. At each

coordinate, almost the entire corpus callosal area spanning 5.0 mm of mediolateral distance for the anterior and middle corpus callosum, and 6.0 mm for the posterior corpus callosum was analyzed. In Figure 1*M–O*, cell density was determined within each segment (500 $\mu$m) of the corpus callosum relative to the distance from the corpus callosal central point, and in Figures 1*D*, 3*E,F*, and 4*B*, the total cell numbers were divided by the total area of the corpus callosum examined. For quantification shown in Fig. 5*B,C*, coronal brain sections +1.0 mm to the bregma were used, which displayed the mediolateral extension of the posterior RMS from the anterior SVZ. In Fig. 5*B*, the distance ($\mu$m) from SVZ dorsal corner to the most laterally positioned EYFP$^+$/GFAP$^+$ cells in the posterior RMS was measured. For each marker, at least 10 sections were analyzed, and cells were identified by their DAPI labeled nuclei.

*Extrapolation of net daily addition of YFP$^+$/GFAP$^+$ astrocytes.* To estimate net daily addition of fate-mapped corpus callosum astrocytes (Fig. 4*D*), net increases in numbers of YFP$^+$/GFAP$^+$ cells in the corpus callosum during the time-intervals between 0 and 40, 40 and 120, and 120 and 270 d post-TM were divided by the number of days spanning the two TM time-points (i.e., 40, 80, 150 d, respectively). Each value in the graph represents the average net daily addition of YFP$^+$/GFAP$^+$ astrocytes between the two post-TM time intervals.

*Statistical analyses.* Data are expressed as mean ± SEM. Statistical analyses were performed by ANOVA with Newman–Keuls *post hoc* testing (using GraphPad Prism 5).

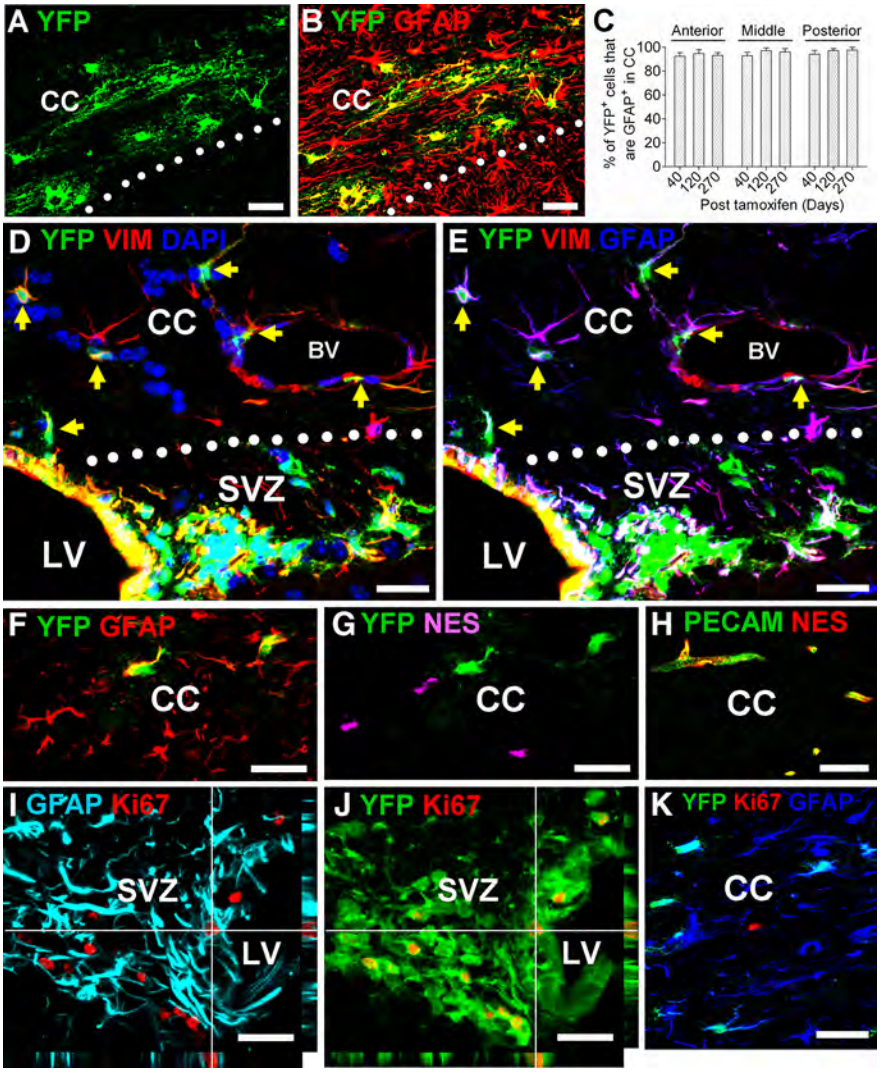


**Figure 2.** Lack of immature properties of nestin fate-mapped astrocytes in the adult corpus callosum. ***A***, ***B***, Images of the posterior corpus callosum at 270 d post-TM immunostained for EYFP and GFAP. ***C***, The percentages of EYFP$^+$ cells that were GFAP$^+$ in the anterior, middle, and posterior corpus callosum, showing that the vast majority of EYFP$^+$ cells were astrocytes. ***D***, ***E***, Images of the middle corpus callosum in close proximity to the SVZ at 120 d post-TM. Arrows indicate EYFP$^+$/vimentin$^+$/GFAP$^+$ cells in the corpus callosum. Note that all EYFP$^+$/vimentin$^+$ cells were also GFAP$^+$ and no EYFP$^+$/vimentin$^+$/GFAP$^-$ cells (i.e., presumably immature astrocytes) were detected in the corpus callosum. ***F***, ***G***, EYFP$^+$/GFAP$^+$ cells in the corpus callosum do not express nestin. ***H***, Colocalization of nestin and PECAM (i.e., endothelial cells) expressions in the corpus callosum of adult wild-type mice. ***I***, ***J***, Orthogonal images of EYFP$^+$/GFAP$^+$/Ki67$^+$ cell in the SVZ at 120 d post-TM, showing the presence of a fate-mapped mitotic astroglial cell (i.e., presumably type B cell). ***K***, EYFP$^+$/GFAP$^+$ astrocytes in the corpus callosum do not proliferate. BV, Blood vessel; CC, corpus callosum; LV, lateral ventricle. Dotted lines in (***A***, ***B***, ***D***, ***E***) demarcate the corpus callosum. Scale bars, 25 $\mu$m. Results are mean ± SEM ($n = 3–4$ brains).

## Results

### Nestin$^+$ SVZ NPCs give rise to astrocytes in the normal adult corpus callosum

To examine SVZ-derived astrogliogenesis in the corpus callosum during normal adulthood, we fate-mapped nestin$^+$ NPCs in the SVZ by administering TM to 3-month-old adult NCER mice. In mice killed 1 d after completing a series of TM administration (i.e., IP, daily injection for 4 consecutive days), fate-mapped (i.e., EYFP$^+$) cells were restricted to the SVZ, and were not detected in neighboring corpus callosum, cortex, or striatum (Fig. 1*A*), confirming a lack of ectopic recombination by nestin-creER$^{T2}$ in these forebrain structures. We then mapped the progeny of EYFP$^+$ cells at later time-points (40, 120 and 270 d post-TM) (Fig. 1*B*). Immunohistochemical analyses were performed in coronal brain sections at three different anterior–posterior coordinates: 1.0 mm anterior, 0.0 mm, and 1.0 mm posterior to the bregma (designated as anterior, middle, and posterior corpus callosum, respectively; Fig. 1*C*). With increasing time post-TM administration, increasing numbers of EYFP$^+$ cells were present in all three examined positions of the corpus callosum (Fig. 1*D–L*). The number of these EYFP$^+$ cells was highest in the posterior and lowest in the anterior corpus callosum. We also quantified mediolateral distributions of EYFP$^+$ cells to determine the extents of their migration with respect to the SVZ (Fig. 1*M–O*). In the anterior and middle corpus callosum, most EYFP$^+$ cells were located in close proximity to the SVZ (Fig. 1*E–H,M,N*), but in the posterior corpus callosum, EYFP$^+$ cells were more widely distributed (Fig. 1*I–L,O*), including EYFP$^+$ cells in the medial corpus callosum, relatively far from the SVZ (Fig. 1*K,L,O*). The vast majority of EYFP$^+$ cells (i.e., 93–97%) in the corpus callosum were GFAP$^+$ (Fig. 2*A–C*), the remainder being GFAP$^-$/Sox10$^+$ oligodendroglial lineage cells or doublecortin (DCX)$^+$ neuroblasts (data not shown). We did not detect fate-mapped endothelial cells (Fig. 3*A–D*) or microglia (data not shown). These results indicated ongoing recruitment of astrocytes from the SVZ to the corpus callosum during normal adulthood.

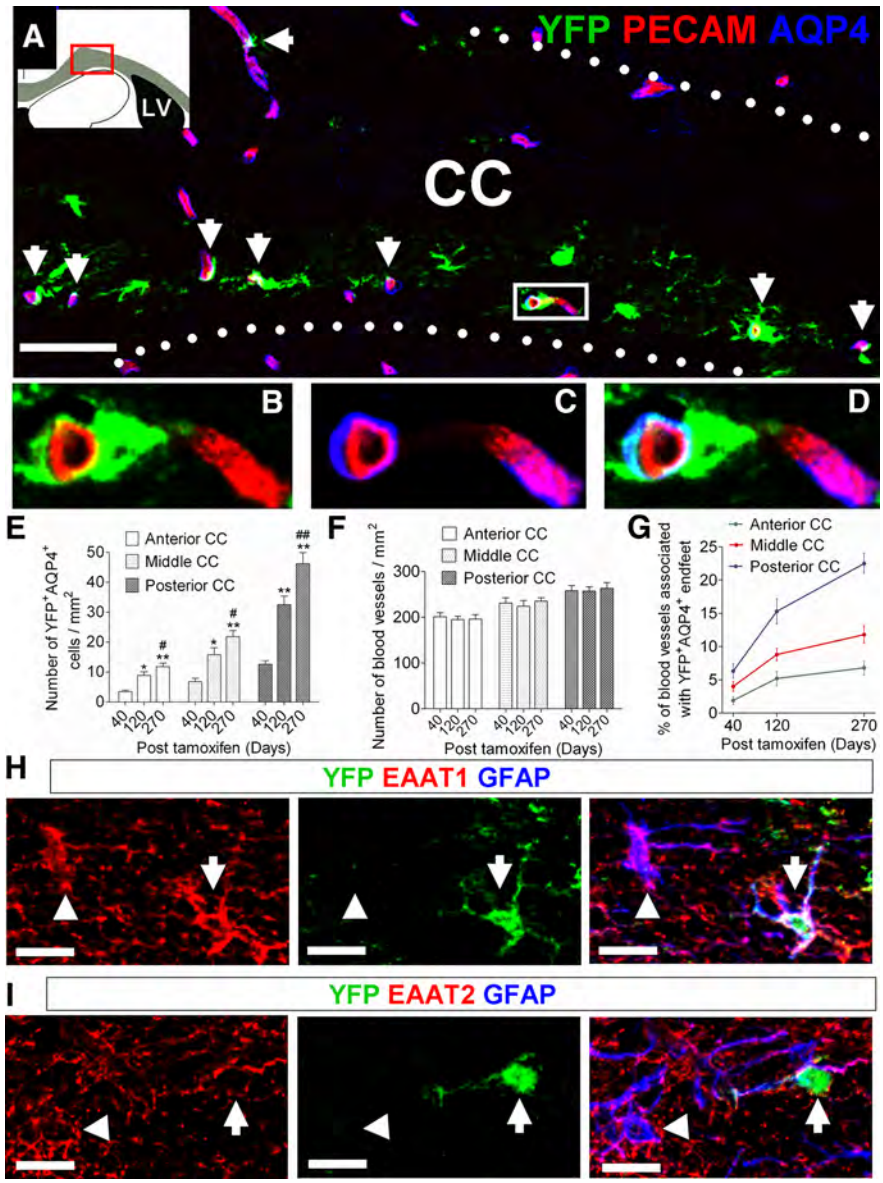


**Figure 3.** Formation of perivascular endfeet and glutamate transporters by nestin fate-mapped astrocytes in the adult corpus callosum. ***A***, Low-magnification image of the posterior corpus callosum at 270 d post-TM immunostained for EYFP, GFAP, and AQP4. A red rectangle in the schematic drawing shows the location of the low-magnification image. Arrows indicate the contacts between EYFP$^+$/AQP4$^+$ astrocytic endfeet and PECAM$^+$ endothelial cells. Dotted lines demarcate the corpus callosum. ***B–D***, Higher magnifications of the area marked by the white rectangle in ***A***, showing EYFP$^+$/AQP4$^+$ astrocytic endfeet completely enwrapping a PECAM$^+$ blood vessel. ***E***, The density of EYFP$^+$/AQP4$^+$ perivascular astrocytes in the adult corpus callosum increased with increasing time after TM and toward more posterior regions of the corpus callosum (anterior CC: *$p < 0.01$ vs 40 d, **$p < 0.005$ vs 40 d, #$p < 0.05$ vs 120 d; middle CC: *$p < 0.01$ vs 40 d, **$p < 0.005$ vs 40 d, #$p < 0.05$ vs 120 d; posterior CC: **$p < 0.005$ vs 40 d, ##$p < 0.01$ vs 120 d). ***F***, The density of PECAM$^+$ blood vessels in different anterior–posterior regions of the adult corpus callosum. ***G***, The percentages of PECAM$^+$ blood vessels that were in contact with EYFP$^+$/AQP4$^+$ endfeet in anterior, middle, and posterior corpus callosum with increasing time after TM. Note that at 270 d after TM, 22.5% of total blood vessels in the posterior corpus callosum were associated with EYFP$^+$/AQP4$^+$ astrocytic endfeet. ***H***, ***I***, Both EYFP$^-$/GFAP$^+$ (arrowheads) and EYFP$^+$/GFAP$^+$ (arrows) astrocytes in the corpus callosum expressed excitatory amino acid transporters 1 (EAAT1; ***H***) and EAAT2 (***I***), astrocyte-specific glutamate transporters. CC, Corpus callosum. Scale bars: ***A***, 100 $\mu$m; ***H***, ***I***, 15 $\mu$m. Results are mean ± SEM ($n = 3$–4 brains).

### Nestin fate-mapped astrocytes in the normal adult corpus callosum do not retain immature astroglial characteristics

We further examined whether these newly recruited corpus callosum GFAP$^+$ cells display an immature astroglial phenotype. Vimentin is expressed by radial glia and immature astrocytes in early development and also by mature astrocytes in adults, preceding GFAP expression during normal astroglial maturation (Schnitzer et al., 1981; Pixley and de Vellis, 1984; Galou et al., 1996). Thus, if EYFP$^+$/vimentin$^+$/GFAP$^-$ cells were present in the corpus callosum, they would presumably represent immature astrocytes. All corpus callosum EYFP$^+$/GFAP$^+$ cells coexpressed vimentin, and we did not detect corpus callosum EYFP$^+$/vimentin$^+$/GFAP$^-$ cells (Fig. 2*D*,*E*). Nestin is another immature astroglial marker during early development, but it is not expressed by normal mature astrocytes (Kálmán and Ajtai, 2001; Sild and Ruthazer, 2011). None of the EYFP$^+$/GFAP$^+$ cells in the corpus callosum we examined expressed immunoreactive nestin (Fig. 2*F*,*G*). We observed abundant nestin$^+$ cells in the adult corpus callosum, but they were PECAM$^+$ endothelial cells (Fig 2*H*). Moreover, EYFP$^+$/GFAP$^+$ cells in the corpus callosum were uniformly Ki67$^-$ (Fig. 2*K*), whereas proliferating fate-mapped astroglial cells (i.e., Ki67$^+$/EYFP$^+$/GFAP$^+$ cells) were detectable in the SVZ (Fig. 2*I*,*J*). Altogether, our data indicate that the fate-mapped GFAP$^+$ cells in the adult corpus callosum are mature, postmitotic astrocytes, and that these fate-mapped astrocytes are derived solely from the SVZ without further expansion by proliferation in the corpus callosum.

### Nestin fate-mapped astrocytes in the normal adult corpus callosum display perivascular phenotype and express glutamate transporters

Some EYFP$^+$ cells in the corpus callosum formed aquaporin-4 (AQP-4)$^+$ perivascular contacts (Nielsen et al., 1997) with PECAM$^+$ blood vessels (Fig. 3*A*–*D*). With increasing time post-TM, the numbers of the corpus callosum EYFP$^+$/AQP-4$^+$ astrocytes progressively increased whereas the total numbers of corpus callosum blood vessels remained constant (Fig. 3*E*–*G*). Virtually all of the EYFP$^+$ astrocytes in the corpus callosum had the "star-like" shape and dense GFAP$^+$ glial filaments typical of white matter fibrous astrocytes (Molofsky et al., 2012), and expressed the astroglial-specific excitatory amino acid transporter EAAT1 (GLAST) and EAAT2 (GLT-1; Rothstein et al., 1994; Chaudhry et al., 1995; Fig. 3*H*,*I*). Notably, immunoreactive intensities for EAAT1 and EAAT2 were comparable between SVZ-derived (i.e., EYFP$^+$/GFAP$^+$) and pre-existing (i.e., EYFP$^-$/GFAP$^+$) astrocytes.

### Astroglial turnover in the normal adult corpus callosum

The total numbers of corpus callosum astrocytes in the interval between 3 and 12 months of age did not alter, as determined by quantification of GFAP:GFP$^+$ cells using GFAP:

GFP transgenic mice (Fig. 4*A*,*B*). Furthermore, albeit at low-frequency, we were able to detect astroglial apoptosis by TUNEL assay in the adult corpus callosum (Fig. 4*C*). Together, our results indicated that astrocyte turnover takes place in the normal adult corpus callosum, with continuous provision of new astrocytes from the SVZ. As shown in Fig. 4*D*, addition of new astrocytes to the corpus callosum was more rapid in young than old mice, and in the posterior than anterior segment of the corpus callosum.

### Robust production of RMS astrocytes from nestin$^+$ SVZ NPCs during normal adulthood

To explore the possibility that new astrocytes also transit from the SVZ to the RMS, we analyzed the appearance of EYFP$^+$/GFAP$^+$ astrocytes at posterior (Fig. 5*A*–*E*) and anterior (Fig. 5*F*–*I*) levels of the RMS as a function of time post-TM. For posterior RMS (pRMS), we used coronal sections at 1.0 mm anterior to the bregma to examine the mediolateral stream of the pRMS that extends from the anterior SVZ. At early time-points post-TM (i.e., 3 d: not shown, 7 d: Fig. 5*D*), EYFP$^+$/GFAP$^+$ astrocytes were largely restricted to the SVZ, with a few present in the pRMS. With increasing time post-TM, there was a lateral stream of EYFP$^+$ cells from the SVZ toward the pRMS (Fig. 5*E*; 120 d post-TM), and an increase in both the lateral migration (Fig. 5*B*) and the density (Fig. 5*C*) of EYFP$^+$/GFAP$^+$ astrocytes within the pRMS. For anterior RMS (aRMS), we analyzed both coronal (Fig. 5*H*,*I*) and sagittal sections (Fig. 5*F*,*G*) at 2.5 mm anterior to the bregma and 0.8 mm lateral to the midline, respectively. At 3 d post-TM, a few EYFP$^+$ cells were present in the aRMS, some of which were also GFAP$^+$ (Fig. 5*F*). By 120 d post-TM, a robust stream of EYFP$^+$ cells had become associated with the aRMS (Fig. 5*G*). Most of these EYFP$^+$ cells were DCX$^+$ neuroblasts (Fig. 5*H*), but the aRMS also contained a substantial number of EYFP$^+$/GFAP$^+$ astrocytes, as seen in both sagittal (Fig. 5*G*) and coronal (Fig. 5*I*) sections. Whereas there were numerous fate-mapped DCX$^+$ neuroblasts and neurons in the granule cell layer (GCL) of the olfactory bulb (data not shown), EYFP$^+$/GFAP$^+$ cells, though migrating to the anterior RMS within the olfactory bulb (Fig. 5*J*,*K*), failed to advance into the olfactory bulb GCL (Fig. 5*L*).

Given prior reports of the presence of GFAP$^+$ astroglial precursors in the RMS (Alonso et al., 2008; Alvarez-Buylla et al.,

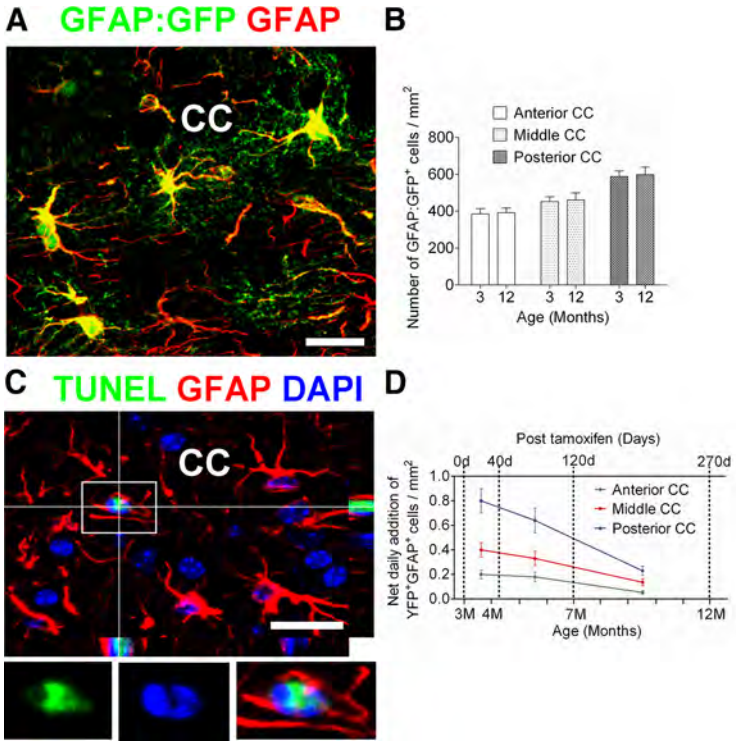


**Figure 4.** Astrocyte turnover in the adult corpus callosum. ***A***, Image of adult GFAP:GFP mouse corpus callosum immunostained for GFP and GFAP showing colocalization of GFAP:GFP and GFAP. ***B***, Quantification of total numbers of GFAP:GFP$^+$ astrocytes in the adult corpus callosum. ***C***, Orthogonal view of a TUNEL$^+$/GFAP$^+$/DAPI$^+$ cell in the adult corpus callosum. Insets below are the magnified images of the area outlined by the rectangle. Note convoluted nucleus with cavitation, a feature of early apoptosis (Johnson et al., 2000). ***D***, Calculated net daily addition of EYFP$^+$/GFAP$^+$ astrocytes in the adult corpus callosum. CC: corpus callosum. Scale bars, 20 $\mu$m. Results are mean ± SEM ($n = 3$ brains in ***B***, $n = 3$–4 brains in ***D***).

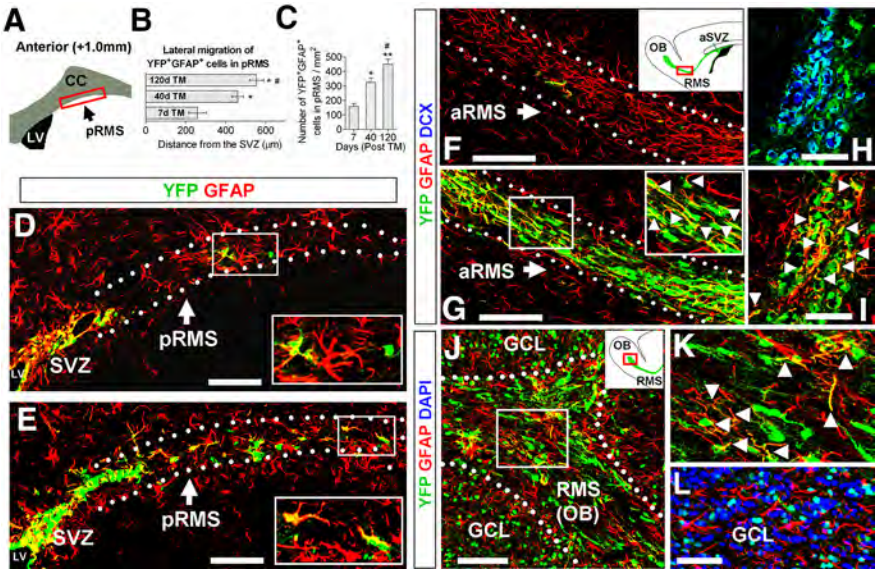


**Figure 5.** Nestin fate-mapping of astrocytes in the adult RMS. ***A***, Schematic representation of a coronal forebrain section 1.0 mm anterior to bregma used for analysis (***B***–***E***) of the posterior RMS (pRMS). With increasing time post-TM, the density of nestin fate-mapped astrocytes (EYFP$^+$/GFAP$^+$) increased in the pRMS, as demonstrated by quantifications (***B***, ***C***) and immunostaining (***D***, 7 d; ***E***, 120 d post-TM). ***F***–***I***, Anterior RMS (aRMS) visualized in sagittal (***F***, ***G***) and coronal (***H***, ***I***) sections. Note the robust stream of SVZ-derived EYFP$^+$ cells in RMS at 120 d post-TM (***G***–***I***). Some of the EYFP$^+$ cells were colabeled with DCX (***H***) or GFAP (***G***, ***I***). Also, note the paucity of EYFP$^+$ cells in the aRMS at 3 d post-TM (***F***), indicating that there were very few nestin$^+$ NPCs in RMS, and validating the mapping strategy. ***J***, ***K***, RMS within the olfactory [RMS(ob)] at 120 d post-TM, showing some fate-mapped cells are astrocytes (EYFP$^+$/GFAP$^+$; ***K***: magnified image of the boxed area in ***J***). ***L***, EYFP$^+$ astrocytes are absent in the GCL at 120 d post-TM. Insets in ***D***, ***E***, and ***G*** are magnified images of the boxed areas. Arrowheads in ***G***, ***I***, and ***K*** indicate fate-mapped astrocytes (EYFP$^+$/GFAP$^+$). The RMS is highlighted by dotted lines. CC, Corpus callosum; LV, lateral ventricle. Scale bars: ***D***–***G***, ***J***, 100 $\mu$m; ***H***, ***I***, ***L***, 50 $\mu$m. *$p < 0.01$ versus 7 d, #$p < 0.05$ versus 40 d in ***B***; *$p <$ 0.01 versus 7 d, **$p < 0.001$ versus 7 d, #$p < 0.01$ versus 40 d in ***C***. Results are mean ± SEM ($n = 3$–4 brains).

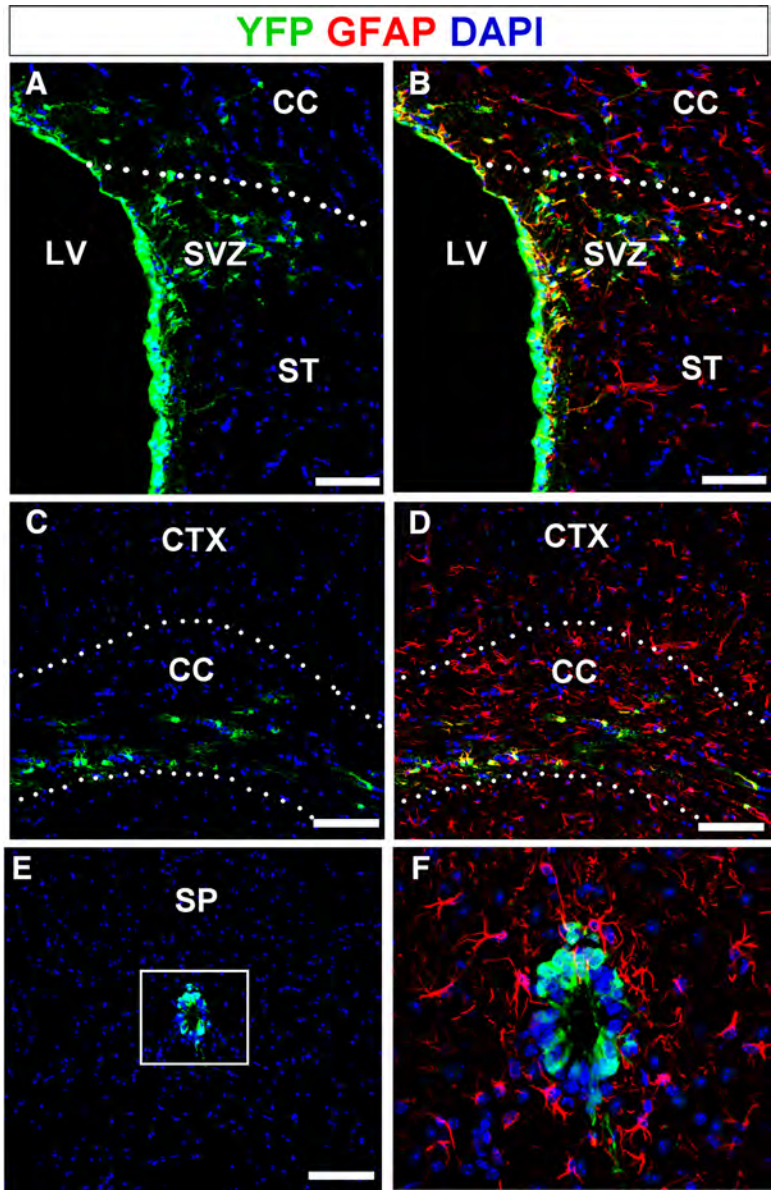


**Figure 6.** Absence of NSC-derived astroglial production in the forebrain gray matter and the spinal cord in normal adults. ***A–D***, Low-magnification images of coronal brain sections at 270 d post-TM. EYFP$^+$/GFAP$^+$ cells migrated into the corpus callosum in both close proximity to the SVZ (***A***, ***B***) and distal to the SVZ (***C***, ***D***), but did not enter the striatum (***A***, ***B***) or cortex (***C***, ***D***). ***E***, The absence of EYFP$^+$ cells outside the central cannel at 270 d post-TM. ***F***, Higher-magnification image of the area outlined by a rectangle in ***E***, showing the lack of NSC-derived astrogliogenesis in the adult spinal cord. CC, Corpus callosum; CTX, cortex; LV, lateral ventricle; SP, spinal cord; ST, striatum. Scale bars, 100 $\mu$m.

2008) and our finding that a few EYFP$^+$/GFAP$^+$ cells were located along the RMS at early days post-TM, we examined proliferation of GFAP$^+$ cells in the adult RMS. No Ki67$^+$/GFAP$^+$ cells were detected in the adult RMS at 3 or 7 months of age, arguing against RMS GFAP$^+$ cells as a substantial source for new astrocyte production in the normal adult RMS.

### Lack of nestin$^+$ NPC-derived astrogliogenesis in the forebrain cortex and striatum, and in the spinal cord during normal adulthood

We observed no fate-mapped astrocytes (i.e., EYFP$^+$/GFAP$^+$) in the normal adult cortex or striatum (Fig. 6*A–D*; 270 d post-TM). In the normal adult spinal cord, EYFP expression was restricted to the central canal, with no fate-mapped GFAP$^+$ astrocytes elsewhere in the spinal cord gray or white matter (Fig. 6*E*,*F*; 270 d post-TM).

## Discussion

The best documented function of nestin$^+$ SVZ NPCs in normal adult mice is the production of neuroblasts; these migrate via the RMS to the olfactory bulb, where they contribute to olfactory learning (Sakamoto et al., 2014). SVZ NPCs also produce oligodendroglial progenitor cells after forebrain demyelination (Menn et al., 2006; Sullivan et al., 2013), and contribute, along with reactive astrocytes in gray and white matter, to forebrain astrogliosis following CNS trauma, ischemia, or inflammation (Buffo et al., 2008; Li et al., 2010; Robel et al., 2011; Benner et al., 2013). So far, evidence of SVZ astrogliogenesis in normal adults has been scant. Prior retroviral lineage tracing studies in the normal adult SVZ extending to 2–3 weeks postinjection (Doetsch et al., 1999; Menn et al., 2006) documented neuronogenesis and oligodendrogenesis, but did not specifically address astrogliogenesis. Interestingly, McCarthy and Leblond (1988) reported that, although a 2 h systemic $^3$H-thymidine pulse failed to label corpus callosum astrocytes in 9 month postnatal mice, 12% of the total corpus callosum astrocytes were labeled following daily systemic administration of $^3$H-thymidine for 30 d. However, this long $^3$H-thymidine-labeling approach was not designed to discriminate between astroglial mitosis in the corpus callosum and mitotic labeling of SVZ progenitor cells that subsequently migrated into the corpus callosum.

In contrast, our long-term nestin fate-mapping approach showed that the SVZ is a source for continuous astrogliogenesis in the normal adult corpus callosum. This conclusion was supported by the absence of Ki67$^+$ (proliferating) fate-mapped astrocytes in the corpus callosum, and the progressive accumulation of fate-mapped corpus callosum astrocytes with increasing time post-TM. These newly recruited corpus callosum astrocytes formed AQP4$^+$-labeled contacts with blood vessels and expressed the glutamate transporters EAAT1 and EAAT2. We did not detect any fate-mapped cells with immature astroglial features in the corpus callosum: all corpus callosum astrocytes, whether EYFP$^+$ or EYFP$^-$, were vimentin$^+$ and no EYFP$^+$/vimentin$^+$/GFAP$^-$ cells (immature astrocytes) were present in the corpus callosum. Furthermore, no corpus callosum EYFP$^+$ astrocytes in these normal adult mice expressed immunoreactive nestin.

Despite the progressive accumulation of EYFP$^+$ astrocytes in the corpus callosum with increasing time post-TM, overall numbers of corpus callosum astrocytes did not increase, and fate-mapped astrocytes did not migrate into the adjacent cortex or

striatum. These observations together with the occasional corpus callosum astroglial apoptosis that we documented strongly suggest ongoing astroglial replacement in the normal adult corpus callosum. Our data (Fig. 4*D*) also indicate that >10% of the corpus callosum astrocytes present in normal 3-month-old mice are replaced by SVZ-derived new astrocytes over the ensuing 9 months.

SVZ NSCs differentiate into astrocytes that, in the early postnatal period, form a glial tube within the RMS (Bonfanti and Peretto, 2007; Nityanandam et al., 2012). However, whether the SVZ continues to produce RMS astrocytes during adulthood has not been determined. Our study shows that some nestin fate-mapped astrocytes, rather than entering the corpus callosum, join the astroglial latticework that outlines the RMS and guides RMS neuroblast migration (Sun et al., 2010). It has been reported that the adult murine RMS contains cells that, by their capacity to generate neurospheres when cultured with epidermal growth factor or fibroblast growth factor-2, can be classified as neural stem cells (Gritti et al., 2002). But because few EYFP$^+$/GFAP$^+$ cells were present in either posterior or anterior RMS in mice killed a week or less post-TM (Fig. 5*D*,*F*), and we saw no Ki67$^+$/GFAP$^+$ cells in the RMS at any time point, we concluded that the fate-mapped astrocytes that accumulated in the RMS at late time-points post-TM originated in the SVZ. These EYFP$^+$/GFAP$^+$ astrocytes were intermingled with DCX$^+$ neuroblasts (Fig. 5*H*,*I*). But unlike the migrating RMS neuroblasts, these fate-mapped astrocytes did not penetrate into the granule cell and periglomerular layers of the olfactory (Fig. 5*L*).

In summary, our data demonstrate for the first time that there is slow, ongoing recruitment of astrocytes originating from nestin$^+$ SVZ NPCs in the normal adult mammalian forebrain. It will be interesting in future to determine the relative contributions of altered rates of SVZ astrogliogenesis and of astroglial apoptosis to forebrain reactive astrogliosis, a feature of many neurodegenerative and neuroinflammatory diseases.

## References


Agrawal HC, Davis JM, Himwich WA (1968) Developmental changes in mouse brain: weight, water content and free amino acids. J Neurochem 15:917–923. CrossRef Medline

Alonso M, Ortega-Pérez I, Grubb MS, Bourgeois JP, Charneau P, Lledo PM (2008) Turning astrocytes from the rostral migratory stream into neurons: a role for the olfactory sensory organ. J Neurosci 28:11089–11102. CrossRef Medline

Alvarez-Buylla A, Kohwi M, Nguyen TM, Merkle FT (2008) The heterogeneity of adult neural stem cells and the emerging complexity of their niche. Cold Spring Harb Symp Quant Biol 73:357–365. CrossRef Medline

Bandeira F, Lent R, Herculano-Houzel S (2009) Changing numbers of neuronal and non-neuronal cells underlie postnatal brain growth in the rat. Proc Natl Acad Sci U S A 106:14108–14113. CrossRef Medline

Benner EJ, Luciano D, Jo R, Abdi K, Paez-Gonzalez P, Sheng H, Warner DS, Liu C, Eroglu C, Kuo CT (2013) Protective astrogenesis from the SVZ niche after injury is controlled by Notch modulator Thbs4. Nature 497:369–373. CrossRef Medline

Bonfanti L, Peretto P (2007) Radial glial origin of the adult neural stem cells in the subventricular zone. Prog Neurobiol 83:24–36. CrossRef Medline

Buffo A, Rite I, Tripathi P, Lepier A, Colak D, Horn AP, Mori T, Götz M (2008) Origin and progeny of reactive gliosis: A source of multipotent cells in the injured brain. Proc Natl Acad Sci U S A 105:3581–3586. CrossRef Medline

Chaudhry FA, Lehre KP, van Lookeren Campagne M, Ottersen OP, Danbolt NC, Storm-Mathisen J (1995) Glutamate transporters in glial plasma membranes: highly differentiated localizations revealed by quantitative ultrastructural immunocytochemistry. Neuron 15:711–720. CrossRef Medline

Chuang N, Mori S, Yamamoto A, Jiang H, Ye X, Xu X, Richards LJ, Nathans J, Miller MI, Toga AW, Sidman RL, Zhang J (2011) An MRI-based atlas and database of the developing mouse brain. Neuroimage 54:80–89. CrossRef Medline

Doetsch F, Caillé I, Lim DA, García-Verdugo JM, Alvarez-Buylla A (1999) Subventricular zone astrocytes are neural stem cells in the adult mammalian brain. Cell 97:703–716. CrossRef Medline

Galou M, Colucci-Guyon E, Ensergueix D, Ridet JL, Gimenez y Ribotta M, Privat A, Babinet C, Dupouey P (1996) Disrupted glial fibrillary acidic protein network in astrocytes from vimentin knockout mice. J Cell Biol 133:853–863. CrossRef Medline

Ge WP, Miyawaki A, Gage FH, Jan YN, Jan LY (2012) Local generation of glia is a major astrocyte source in postnatal cortex. Nature 484:376–380. CrossRef Medline

Gritti A, Bonfanti L, Doetsch F, Caille I, Alvarez-Buylla A, Lim DA, Galli R, Garcia Verdugo JM, Herrera DG, Vescovi AL (2002) Multipotent neural stem cells reside into the rostral extension and olfactory bulb of adult rodents. J Neurosci 22:437–445. Medline

Johnson VL, Ko SC, Holmstrom TH, Eriksson JE, Chow SC (2000) Effector caspases are dispensable for the early nuclear morphological changes during chemical-induced apoptosis. J Cell Sci 113:2941–2953. Medline

Kálmán M, Ajtai BM (2001) A comparison of intermediate filament markers for presumptive astroglia in the developing rat neocortex: immunostaining against nestin reveals more detail, than GFAP or vimentin. Int J Dev Neurosci 19:101–108. CrossRef Medline

Lagace DC, Whitman MC, Noonan MA, Ables JL, DeCarolis NA, Arguello AA, Donovan MH, Fischer SJ, Farnbauch LA, Beech RD, DiLeone RJ, Greer CA, Mandyam CD, Eisch AJ (2007) Dynamic contribution of nestin-expressing stem cells to adult neurogenesis. J Neurosci 27:12623–12629. CrossRef Medline

Levison SW, Chuang C, Abramson BJ, Goldman JE (1993) The migrational patterns and developmental fates of glial precursors in the rat subventricular zone are temporally regulated. Development 119:611–622. Medline

Li L, Harms KM, Ventura PB, Lagace DC, Eisch AJ, Cunningham LA (2010) Focal cerebral ischemia induces a multilineage cytogenic response from adult subventricular zone that is predominantly gliogenic. Glia 58:1610–1619. CrossRef Medline

Ling EA, Leblond CP (1973) Investigation of glial cells in semithin sections: II. Variation with age in the numbers of the various glial cell types in rat cortex and corpus callosum. J Comp Neurol 149:73–81. CrossRef Medline

McCarthy GF, Leblond CP (1988) Radioautographic evidence for slow astrocyte turnover and modest oligodendrocyte production in the corpus callosum of adult mice infused with 3H-thymidine. J Comp Neurol 271:589–603. CrossRef Medline

Menn B, Garcia-Verdugo JM, Yaschine C, Gonzalez-Perez O, Rowitch D, Alvarez-Buylla A (2006) Origin of oligodendrocytes in the subventricular zone of the adult brain. J Neurosci 26:7907–7918. CrossRef Medline

Molofsky AV, Krenick R, Ullian E, Tsai HH, Deneen B, Richardson WD, Barres BA, Rowitch DH (2012) Astrocytes and disease: a neurodevelopmental perspective. Genes Dev 26:891–907. CrossRef Medline

Nielsen S, Nagelhus EA, Amiry-Moghaddam M, Bourque C, Agre P, Ottersen OP (1997) Specialized membrane domains for water transport in glial cells: high-resolution immunogold cytochemistry of aquaporin-4 in rat brain. J Neurosci 17:171–180. Medline

Nityanandam A, Parthasarathy S, Tarabykin V (2012) Postnatal subventricular zone of the neocortex contributes GFAP+ cells to the rostral migratory stream under the control of Sip1. Dev Biol 366:341–356. CrossRef Medline

Pixley SK, de Vellis J (1984) Transition between immature radial glia and mature astrocytes studied with a monoclonal antibody to vimentin. Brain Res 317:201–209. Medline

Robel S, Berninger B, Götz M (2011) The stem cell potential of glia: lessons from reactive gliosis. Nat Rev Neurosci 12:88–104. CrossRef Medline

Rothstein JD, Martin L, Levey AI, Dykes-Hoberg M, Jin L, Wu D, Nash N, Kuncl RW (1994) Localization of neuronal and glial glutamate transporters. Neuron 13:713–725. CrossRef Medline

Sakamoto M, Ieki N, Miyoshi G, Mochimaru D, Miyachi H, Imura T, Yamaguchi M, Fishell G, Mori K, Kageyama R, Imayoshi I (2014) Continuous postnatal neurogenesis contributes to formation of the olfactory bulb neural circuits and flexible olfactory associative learning. J Neurosci 34: 5788–5799. CrossRef Medline

Sauvageot CM, Stiles CD (2002) Molecular mechanisms controlling cortical gliogenesis. Curr Opin Neurobiol 12:244–249. CrossRef Medline

Schnitzer J, Franke WW, Schachner M (1981) Immunocytochemical demonstration of vimentin in astrocytes and ependymal cells of developing and adult mouse nervous system. J Cell Biol 90:435–447. CrossRef Medline

Sild M, Ruthazer ES (2011) Radial glia: progenitor, pathway, and partner. Neuroscientist 17:288–302. CrossRef Medline

Sohn J, Selvaraj V, Wakayama K, Orosco L, Lee E, Crawford SE, Guo F, Lang J, Horiuchi M, Zarbalis K, Itoh T, Deng W, Pleasure D (2012) PEDF is a novel oligodendrogenic morphogen acting on the adult SVZ and corpus callosum. J Neurosci 32:12152–12164. CrossRef Medline

Srinivas S, Watanabe T, Lin CS, William CM, Tanabe Y, Jessell TM, Costantini F (2001) Cre reporter strains produced by targeted insertion of EYFP and ECFP into the ROSA26 locus. BMC Dev Biol 1:4. CrossRef Medline

Sullivan GM, Mierzwa AJ, Kijpaisalratana N, Tang H, Wang Y, Song SK, Selwyn R, Armstrong RC (2013) Oligodendrocyte lineage and subventricular zone response to traumatic axonal injury in the corpus callosum. J Neuropathol Exp Neurol 72:1106–1125. CrossRef Medline

Sun W, Kim H, Moon Y (2010) Control of neuronal migration through rostral migratory stream in mice. Anat Cell Biol 43:269–279. CrossRef Medline

Suzuki SO, Goldman JE (2003) Multiple cell populations in the early postnatal subventricular zone take distinct migratory pathways: a dynamic study of glial and neuronal progenitor migration. J Neurosci 23:4240–4250. Medline

Zhuo L, Sun B, Zhang CL, Fine A, Chiu SY, Messing A (1997) Live astrocytes visualized by green fluorescent protein in transgenic mice. Dev Biol 187: 36–42. CrossRef Medline

Zimmerman L, Parr B, Lendahl U, Cunningham M, McKay R, Gavin B, Mann J, Vassileva G, McMahon A (1994) Independent regulatory elements in the nestin gene direct transgene expression to neural stem cells or muscle precursors. Neuron 12:11–24. CrossRef Medline